Supporting Information

Linker Desymmetrisation Directs Low-polar Cages in an Anion-Pillared MOF for Acetylene and Ethylene Purification from Ternary Mixtures

Jun-Jie Wu[a], Peng-Dan Zhang[a,c,*], Xue-Qian Wu[a,*], Shuai-Hao Huang[a], Wen-Wen Dong[a], Ya-Pan Wu[a], Dong-Sheng Li[a,b,*]

[a]College of Materials and Chemical Engineering, China Three Gorges University, Yichang 443002, P. R. China.

[b]Hubei Three Gorges Laboratory, Yichang 443007, Hubei, P. R. China.

[c]College of Hydraulic & Environmental Engineering, China Three Gorges University, Yichang 443002, P. R. China.

*Corresponding Author(s): Peng-Dan Zhang: dana929@163.com; Xue-Qian Wu: wuxueqiansnail@163.com, Dong-Sheng Li: lidongsheng1@126.com.

Experimental procedures

Materials synthesis

All the chemicals essential for the experiments were purchased conveniently from the market and used directly without any further purification. Powder X-ray diffraction (PXRD) patterns were obtained via a Rigaku Ultima IV X-ray powder diffractometer with CuKα radiation, (λ = 1.5406 Å) at room temperature (RT). The thermal stability research was conducted on a TGA-50 thermal analyzer with a heating rate of 10 °C min^{-1} under Air atmosphere.

Synthesis of CTGU-45.

Crystalline CTGU-45 was synthesized through solvothermal reaction method. $Cu(AC)_2 \cdot H_2O$ (20.0 mg, 0.6 mmol), TIB ligand (13.8 mg, 0.15 mmol) were dissolved in a solvent mixture of 1 mL of N, N-Dimethylacetamide (DMA), 3 mL of H_2O, 0.3 mL of HBF_4 (37 wt%). The above solution was then transferred and sealed in a 25 mL glass tube, at a 373 K oven for 24 h. After being cooled naturally to room temperature, granular blue crystals of CTGU-45 were obtained through washing several times with DMA and MeOH (yield: about 50% based on $Cu(AC)_2 \cdot H2O$).

Single crystal X-ray diffraction analysis

Single crystal X-ray diffraction (SCXRD) analysis was carried out on a Rigaku Supernova CCD diffractometer equipped with a mirror monochromated enhanced Cu-*Kα* radiation (λ = 1.54184 Å) at 296 K. Using SHELXTL and Olex2 software package, the structure was solved by ShelXT solution program with the intrinsic phasing method and refined by full-matrix least-squares on F^2 with anisotropic displacement.[1-2] Hydrogen atoms of the framework were calculated in ideal positions with isotropic displacement parameters. The guest molecules were highly disordered and could not be

modeled properly, and the residual electron densities resulting from them were removed by the SQUEEZE routine in PLATON (the details were appended in the CIF file). Crystallographic data for CTGU-45 have been deposited in the Cambridge Crystallographic Data Centre (CCDC number: 2522768). These data can be obtained free of charge via deposit@ccdc.cam.ac.uk. Selected crystal parameters and structure refinement details are listed in Table S1.

Table S1. Crystal data and structure refinements for SIFSIX-TPT-Cu 、CTGU-45, and SIFISX-TPA-Cu

Name	SIFSIX-TPT-Cu	CTGU-45	SIFISX-TPA-Cu
Empirical formula	C_{160} H_{112} Cu_6 F_{18} N_{32} Si_3	$C_{20}H_{12}CuF_6N_8Si$	$C_{120}H_{96}Cu_6F_{36}N_{32}Si_6$
Formula weight	3290.32	570.01	3220.03
Temperature/K	446(2)	296(1)	100.00(18)
Crystal system	Cubic	Cubic	Cubic
Space group	*Pm-3*	*Pm-3n*	*Pm-3n*
a (Å)	21.1882(4)	16.1908(2)	17.5176 (2)
b (Å)	21.1882(4)	16.1908(2)	17.5176 (2)
c (Å)	21.1882(4)	16.1908(2)	17.5176 (2)
α (°)	90	90	90
β(°)	90	90	90
γ(°)	90	90	90
Volume (Å^3)	9512.2(5)	4244.29(9)	5375.56 (18)
Z	1	6	1
ρ_{calc} (g cm^{-3})	0.574	1.338	0.995
μ/mm^{-1}	0.743	2.066	1.58
Reflections collected	37996	4734	4435
Independent data	1866	803	982
R_{int}	0.1166	0.0608	0.0297
Goodness-of-fit on F^2	2.772	1.125	1.080
[a]R_1 (I >2σ(I))	0.1701	0.239	0.0395
[a]R_1 (all data)	0.1950	0.0959	0.0474,

[a] $R_1 = \sum||F_o|-|F_c||/\sum|F_o|$.

Static single-component gas adsorption measurements

Before single-component gas adsorption measurements, about 100 mg crystalline samples of CTGU-45 were soaked in 20 mL DMA for 24 h at room temperature. The sample was then immersed in 40 mL of methanol and sealed in a 100 mL glass bottle (fresh methanol was changed every 12 h). Finally, the sample obtained from the previous step was transferred into dichloromethane (20 mL) for another 16 h (fresh solvents were changed every 8 h). After the solvent exchange process was completed, the sample was loaded in a sample tube and further activated under high vacuum at an optimized temperature of 80 ^{o}C for 6 h. Bath temperatures of 298 and 308 K were precisely controlled with a recirculating control system containing a mixture of ethylene glycol and water. The lower temperatures (77 and 273 K) were controlled by a Dewar filled with liquid N_2, and ice-water mixture, respectively.

Kinetic adsorption measurement

The time-dependent adsorption profiles were measured on BSD-DVS dynamic vapor/gas sorption analyzer. About 800 mg crystalline samples of CTGU-45 were loaded into the sample chamber after the solvent exchange process was completed and activated at 100 °C under N_2 flow (200 mL min^{-1}) for 12 h. After being cooled to 25 °C, a single-component gas of C_2H_2, C_2H_4, C_2H_6, CO_2 and CH_4 was introduced into the chamber with a flow rate of 200 mL min^{-1}. The mass of the sample loaded with gas molecules was continuously recorded till adsorption reached equilibrium.

Diffusion time constant

The ratio D' (Dc/r_c^2) is known as the diffusion time constant. It can be further derived from the following micropore diffusion model eq (1). D' can be obtained from the square of the slope (m_t /m_∞ plotted against $\sqrt{t}$) multiplied by

$$\frac{m_t}{m_\infty} \approx \frac{6}{r_c}\sqrt{\frac{D_c t}{\pi}}\left(\frac{m_t}{m_\infty} < 0.3\right) \quad (1)$$

where m_t is the gas uptake at time t，m_∞ is the gas uptake at equilibrium，D_c is the intracrystalline diffusivity of gas molecules in porous media, and r_c is the radius of the equivalent spherical particle.

Kinetic selectivity

The kinetic selectivity (a_{ij}) is defined as

$$a_{ij} = D'_t/D'_j \quad (2)$$

a_{ij} represents the kinetic selectivity based on diffusion rates of the gas molecules and can be obtained from the ratio of diffusion time constant D' , D' can be further derived from the micropore diffusion model eq(1).

Dynamic breakthrough experiments

Practical gas separation experiments were performed using dynamic breakthrough equipment (BSD-MAB) for the binary C_2H_2/CO_2(50/50,v/v)，$C_2H_2/CO_2/CH_4$ (33.33/33.33/33.33, v/v/v), C_2H_6/C_2H_4 (50/50, 10/90, v/v), C_2H_2/C_2H_4 (50/50, 10/90, v/v), and ternary $C_2H_2/C_2H_6/C_2H_4$ (1/10/89, v/v/v/v) gas mixtures at 100 kPa and 298 K. Breakthrough experiments were then carried out in a 6 mm diameter glass column of 100 mm length packed with activated CTGU-45, in which C_2H_2/CO_2, C_2H_6/C_2H_4, C_2H_2/C_2H_4，$C_2H_2/CO_2/CH_4$, $C_2H_2/C_2H_6/C_2H_4$ gas mixture flowed with various total flow rates (4 , 1 , 1 , 6 and 15 mL min^{-1}) at 298 K and 1.0 bar. The adsorption column was heated at 80 ^oC for 6 h under a flow of He (20 mL min^{-1}) for complete activation before the measurement. The gas compositions at the

outlet were determined continuously by mass spectrometry (MS). After the contents of outlet gas reached equilibrium, the saturated adsorption bed was regenerated by He flow (10 mL min^{-1}) for 120 min at 298 K.

Analysis of single-component adsorption isotherms

The single-component adsorption isotherms of C_2H_2, C_2H_4, C_2H_6, CO_2 and CH_4 in CTGU-45 were fitted using the single-site/dual-sites Langmuir-Freundlich models[3].

$$N = A_1 \times \frac{b_1 P^{c_1}}{1 + b_1 P^{c_1}} + A_2 \times \frac{b_2 P^{c_2}}{1 + b_2 P^{c_2}} \quad (3)\ (A_2 = 0, \text{ single-site model})$$

Here N is the adsorption amount in cm^3/g, P is the pressure of the bulk gas at equilibrium with the adsorbed phase (bar), A_1 and A_2 are the saturation loadings of sites A and B (cm^3/g), b_1 and b_2 are the affinity coefficients of sites A and B (1/bar), C_1 and C_2 represent the deviations from an ideal homogeneous surface. The fitting parameters of equation (1) for C_2H_2 , C_2H_4, C_2H_6 , CH_4 and CO_2 are listed in the table (inset: Figure S18-S22). The adsorption selectivity for C_2H_2/CO_2, C_2H_2/CH_4, C_2H_2/C_2H_4 and C_2H_6/C_2H_4 separation was defined by the following equation[4]:

$$S_{1,2} = \frac{q_1/q_2}{P_1/P_2} \quad (4)$$

Here q_1 and q_2 are the equilibrated adsorption molar loading of component 1 and 2 respectively, p_1 and p_2 represent the partial pressure of component 1 and 2 in bulk gas phase.

Calculation of isosteric heat of adsorption (Q_{st})

A virial-type equation comprising of the temperature-independent parameters a_i and b_j was employed to calculate the enthalpies of adsorption for C_2H_2 , C_2H_4 , C_2H_6 , CH_4 and CO_2 in CTGU-45, which measured at 273 ,

283 and 298 K[5].

$$\ln P = \ln N + \frac{1}{T}\sum_{i=0}^{m} a_i N^i + \sum_{j=0}^{n} b_j N^i \quad (5)$$

$$Q_{st} = -R\sum_{i=0}^{m} a_i N^i \quad (6)$$

Here, P is the pressure expressed in mmHg, T is the temperature in K, a_i and b_j are virial coefficients, N is the adsorption amount in mg/g and m/n represent the number of coefficients used to describe the adsorption curves. Q_{st} is coverage-dependent enthalpy of adsorption and R is the universal gas constant.

Dispersion-corrected density functional theory (DFT-D) calculations

Theoretical calculations based on the density functional theory (DFT) were conducted using the Dmol[3] module implemented in the Materials Studio software[6]. Van der Waals interactions were illustrated by the calculation with a semiempirical addition of dispersive forces to the conventional DFT (DFT-D3)[7]. Electron-ion interactions were described using the DFT Semi-core Pseudopots pseudopotentials (DSPP). A double numerical polarized (DNP) basis set was employed to expand the wave functions with an orbital cutoff of 5.2 Å. For the electron-electron exchange and correlation interactions, a generalized gradient approximation (GGA) with Perdew-Burke-Ernzerhof (PBE) exchange-correlation was utilized[8]. The convergence criterion for the electronic self-consistent field (SCF) loop and the total energy convergence criterion were set to be 10^{-6} and 10^{-5} (eV atom^{-1}), respectively. The structure of CTGU-45 and isolated gas molecules placed in a supercell (with the same cell dimensions as the MOF adsorbent) were also optimized as references. The static binding energy (T= 0 K) was then calculated using E_B = E (MOF) + E (gas) – E (MOF+gas). In order to gain the initial positions of the gas molecules within the pore structure, GCMC simulations were carried out firstly by

SORPTION code embedded in the MS.[6] The dispersive and steric repulsive interactions of each atom in CTGU-45 framework and C_2H_2/C_2H_4/C_2H_6/CO_2/CH_4 adsorbates were both modeled by the universal force field (UFF), which has been widely applied in the molecular simulations for MOFs.[9] The QEq method was used to equilibrate and redistribute the overall charge of atoms of the MOF structure, while the charge distribution situation for C_2H_2/C_2H_4/C_2H_6/CO_2/CH_4 molecules was calculated through DFT (ESP). Electrostatic interaction was evaluated through Ewald summation method. The cutoff distance was set at 18.5 Å. 20000000 Monte Carle steps were constructed to simulate the favorable adsorption sites under a fixed pressure, in which the first 10000000 steps were for equilibration and the remains were production steps.

Table S2. IAST selectivity and separation coefficient of CTGU-45 for C_3H_6/C_2H_4

Molecule	Molecular dimensions (Å^3)	Kinetic diameter (Å)	Quadrupole moments (×10^{-26} esu cm^2)	Polarizability (×10^{-25} cm^3)	Boiling point (K)
CH_4	3.7 × 3.7 × 3.7	3.76	0	25.9	111.6
CO_2	3.2 × 3.3 × 5.4	3.3	-4.3	29.1	194.7
C_2H_2	3.3 × 3.3 × 5.7	3.3	7.5	33.3-39.3	189.3
C_2H_4	3.3×4.2×4.8	4.2	1.5	42.5	169.4
C_2H_6	3.8×4.1×4.8	4.4	0.65	44.3-44.7	184.5

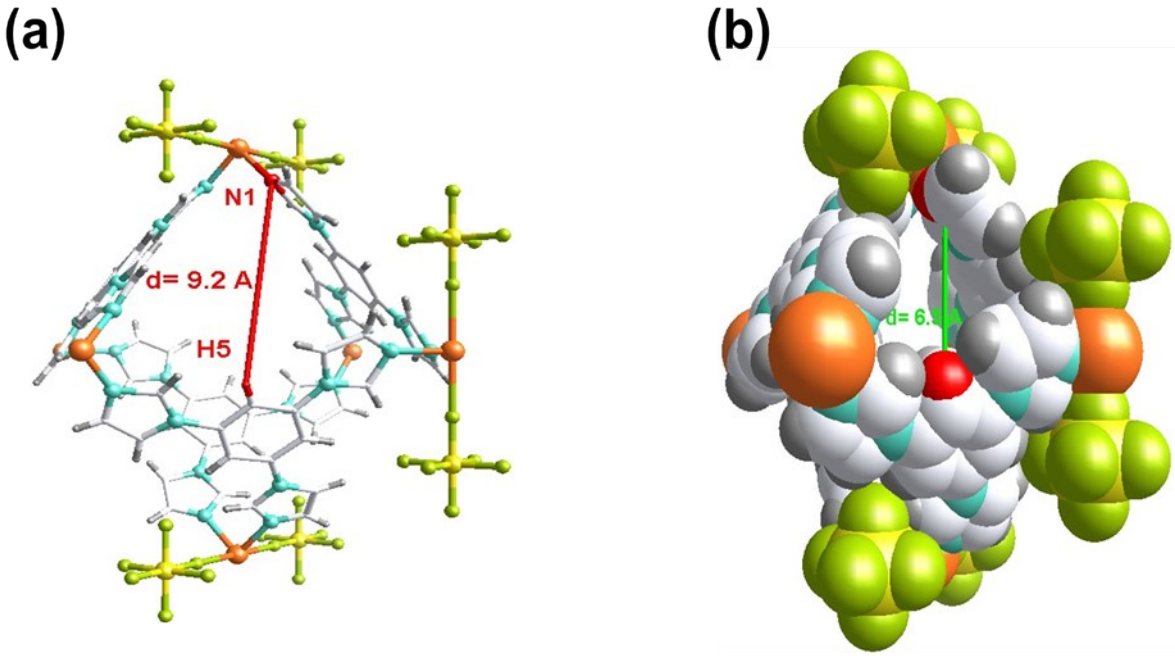

Figure S1. Estimation of Window Aperture in CTGU-45. Due to the irregular window geometry, the effective aperture size is estimated from the H5···N1 distance (ca. 9.2 Å). Subtracting the van der Waals radii of H (1.20 Å) and N (1.55 Å) yields an effective aperture of ca. 6.5 Å. (a) Including atomic radii. (b) Excluding atomic radii.

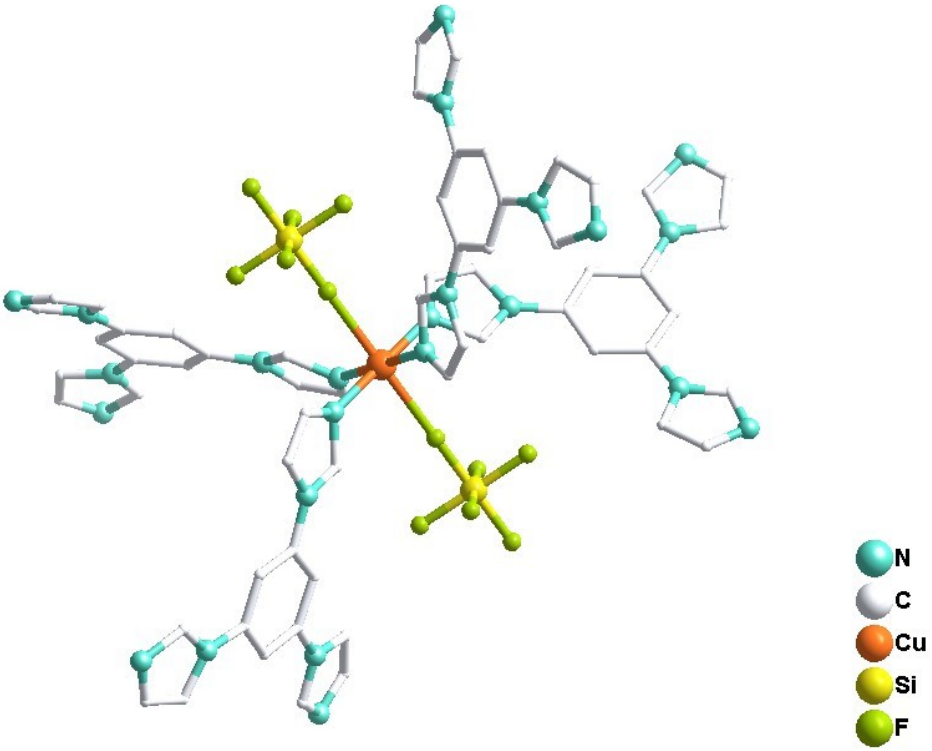

Figure S2. The basic coordination environment of CTGU-45.

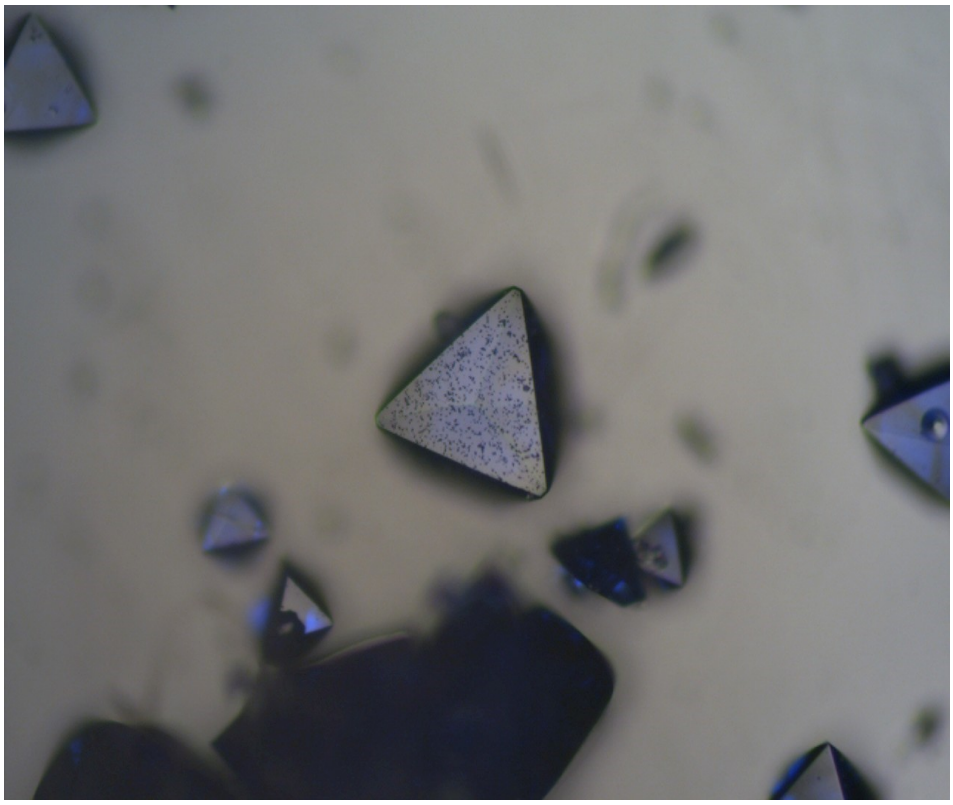

Figure S3. Photograph of freshly prepared CTGU-48 crystals.

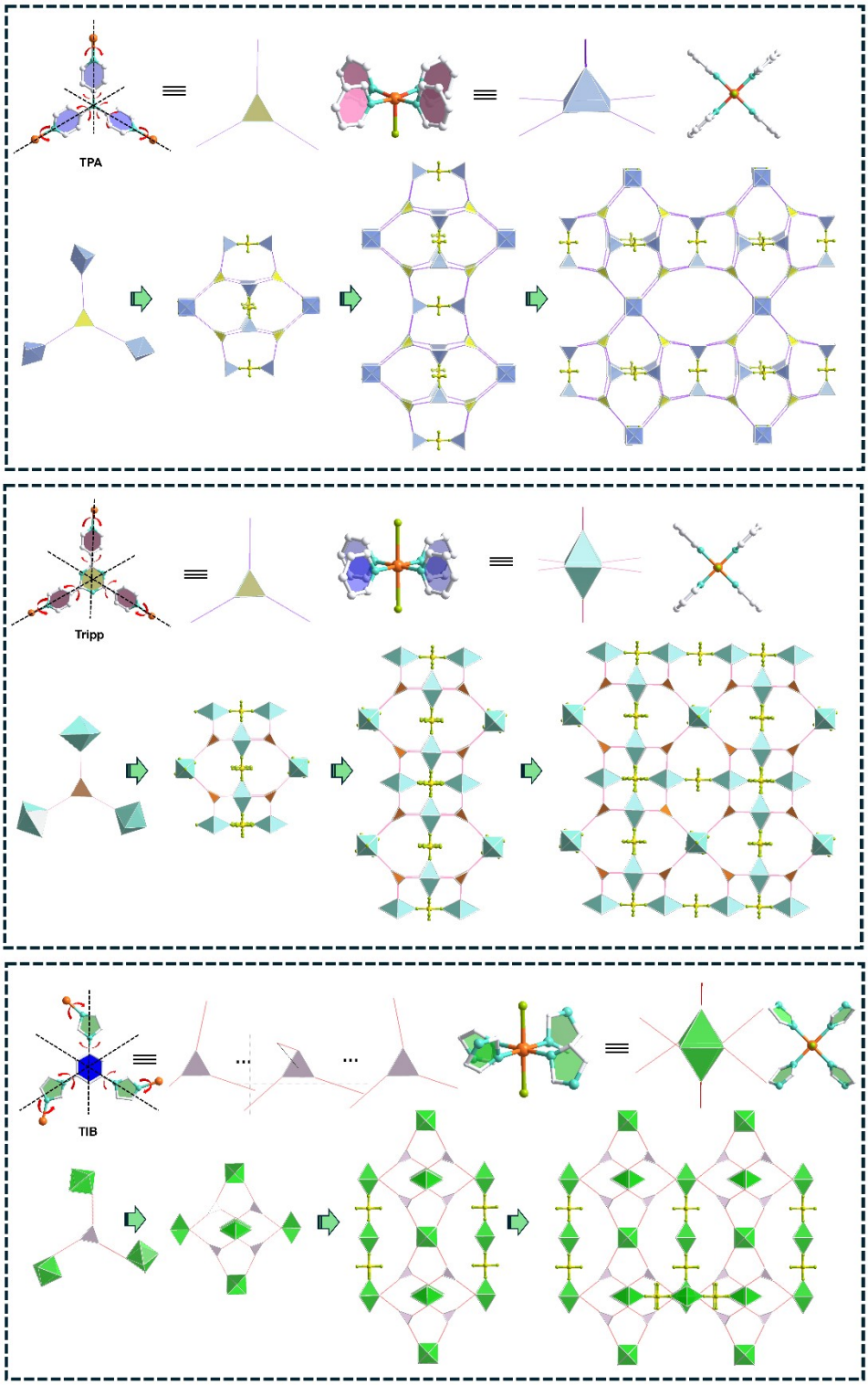

Figure S4. Topological evolution analysis for SIFSIX-Cu-TPA, Tripp-Cu-SIFSIX, and CTGU-45.

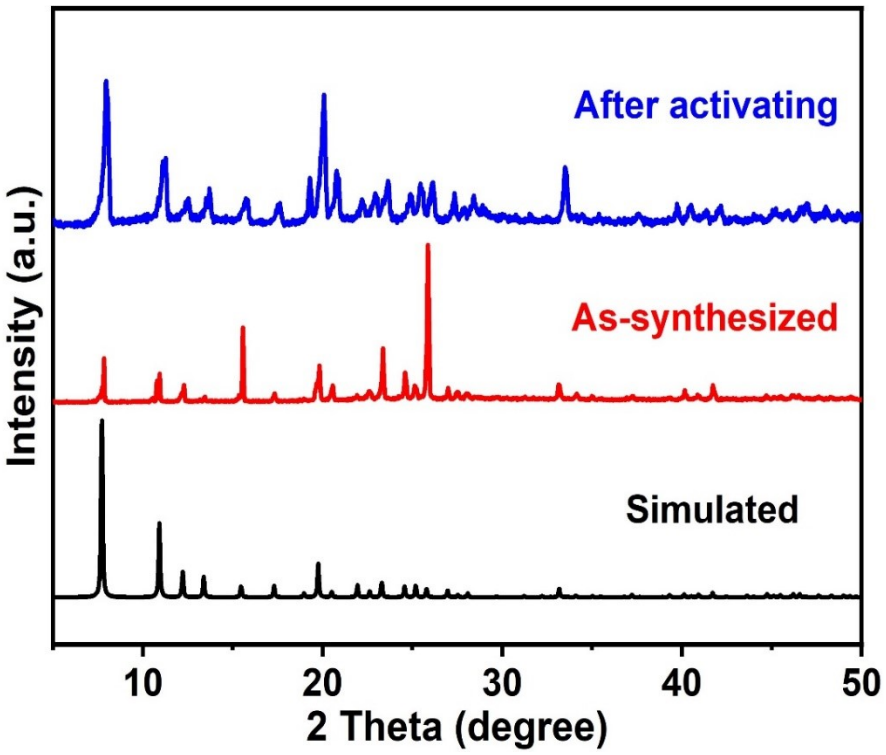

Figure S5. The PXRD patterns of freshly prepared/activated CTGU-45, and the simulated patterns based on SCXRD data.

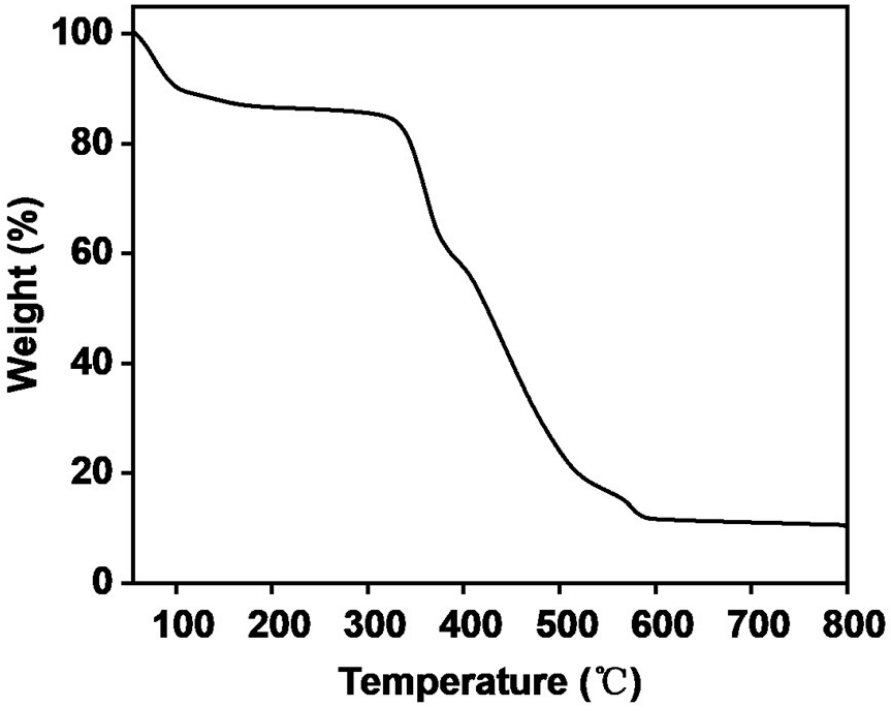

Figure S6. Thermogravimetric curves of CTGU-45 measured under air atmosphere.

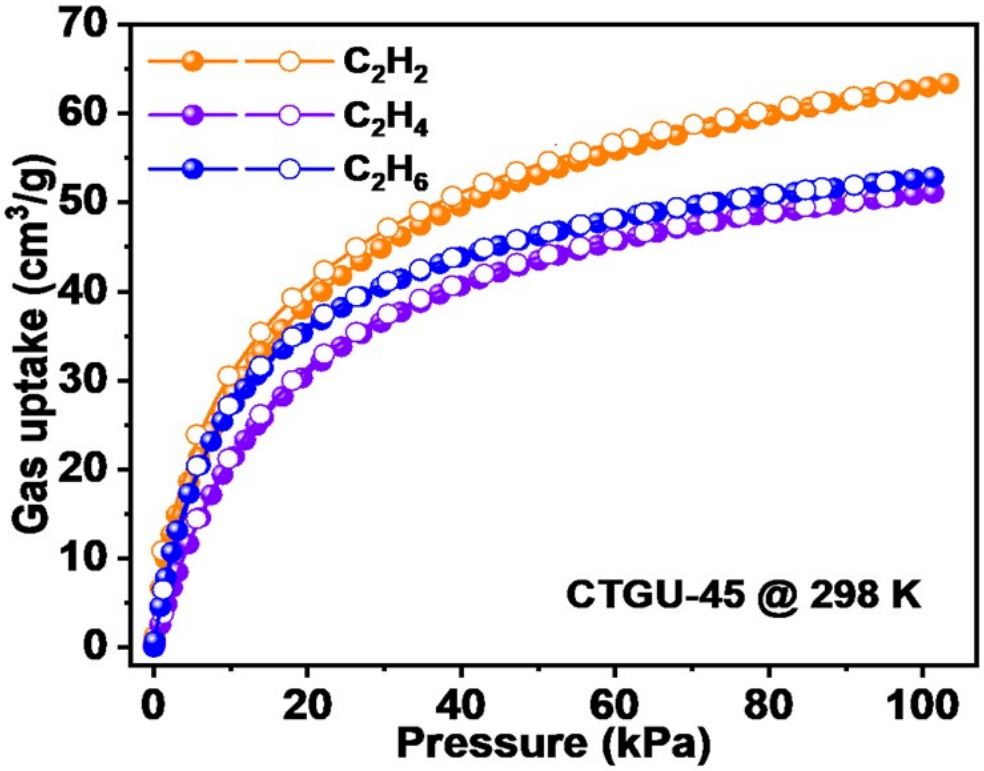

Figure S7. The adsorption isotherms of C_2H_2, C_2H_4, C_2H_6 in CTGU-45 at 298 K.

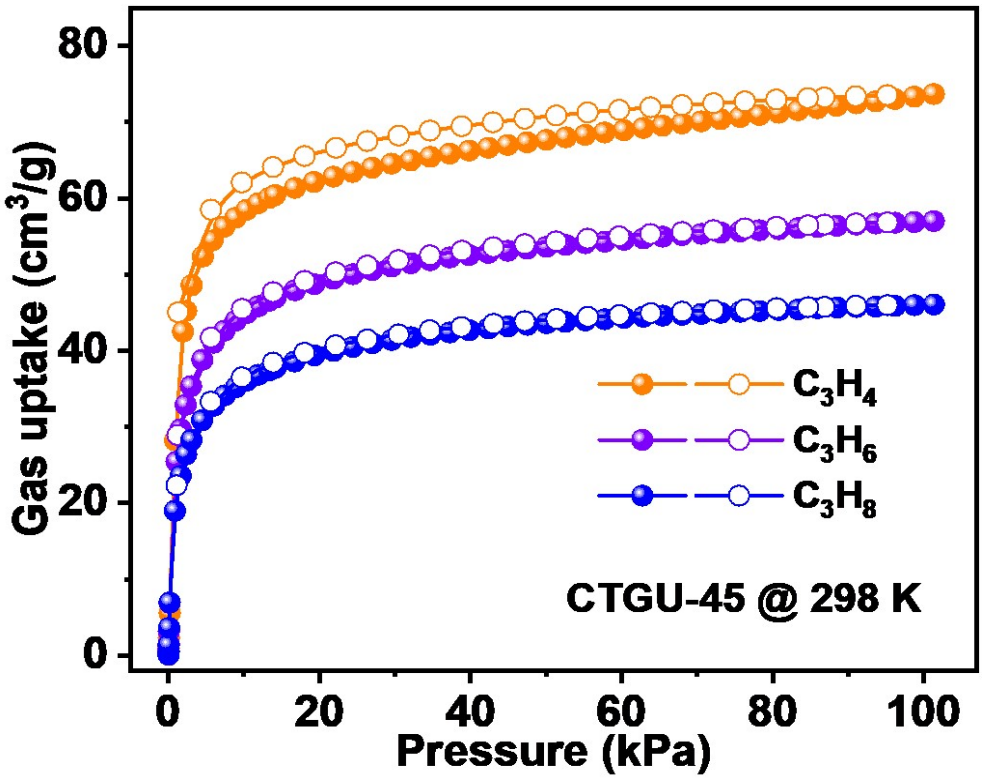

Figure S8. The adsorption isotherms of C_3H_4, C_3H_6 and C_3H_8 in CTGU-45 at 298 K.

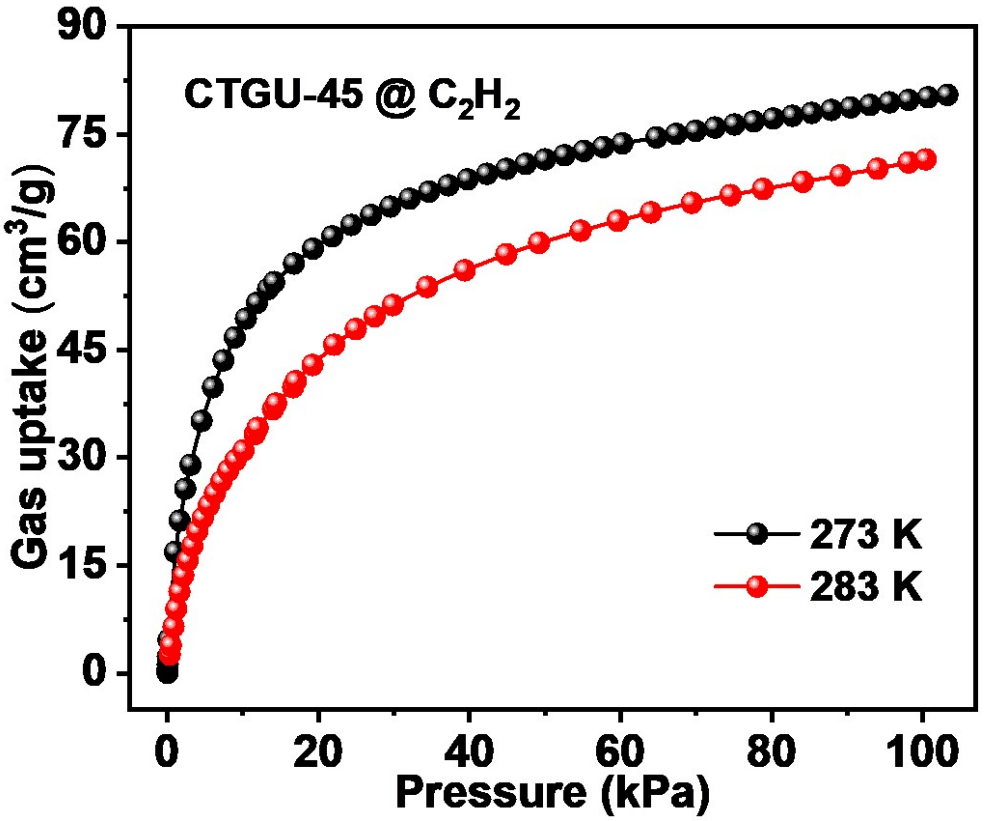

Figure S9. The adsorption isotherms of C_2H_2 in CTGU-45 at 273 , 283 K.

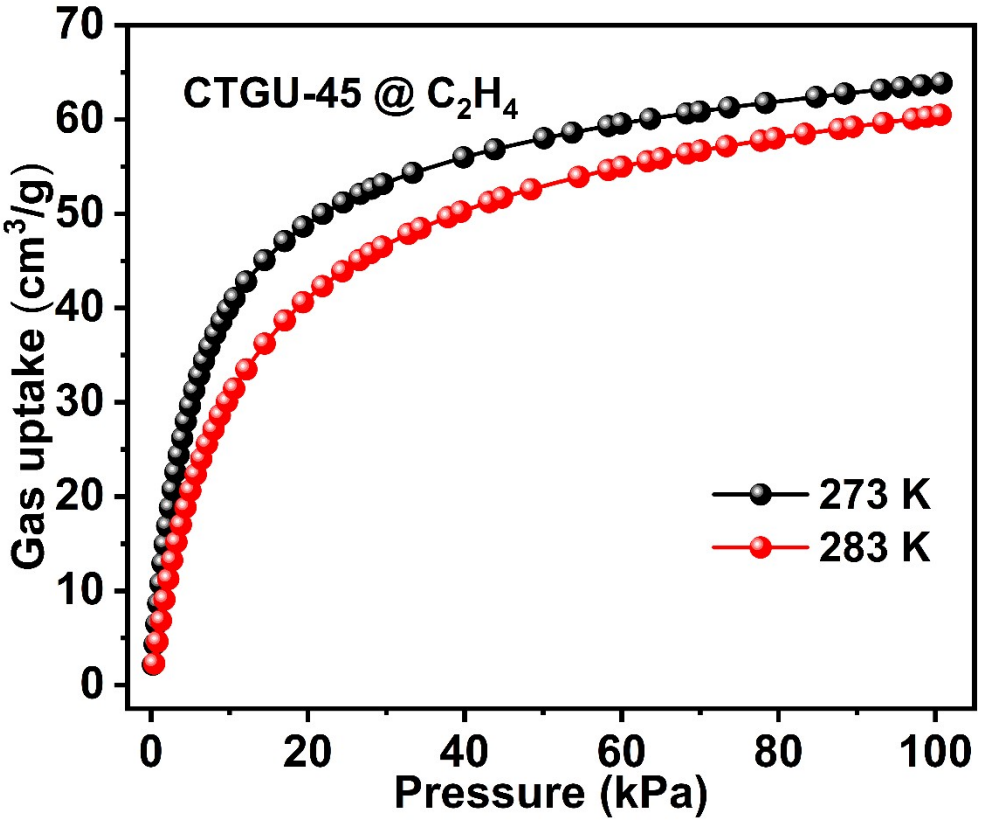

Figure S10. The adsorption isotherms of C_2H_4 in CTGU-45 at 273 , 283 K.

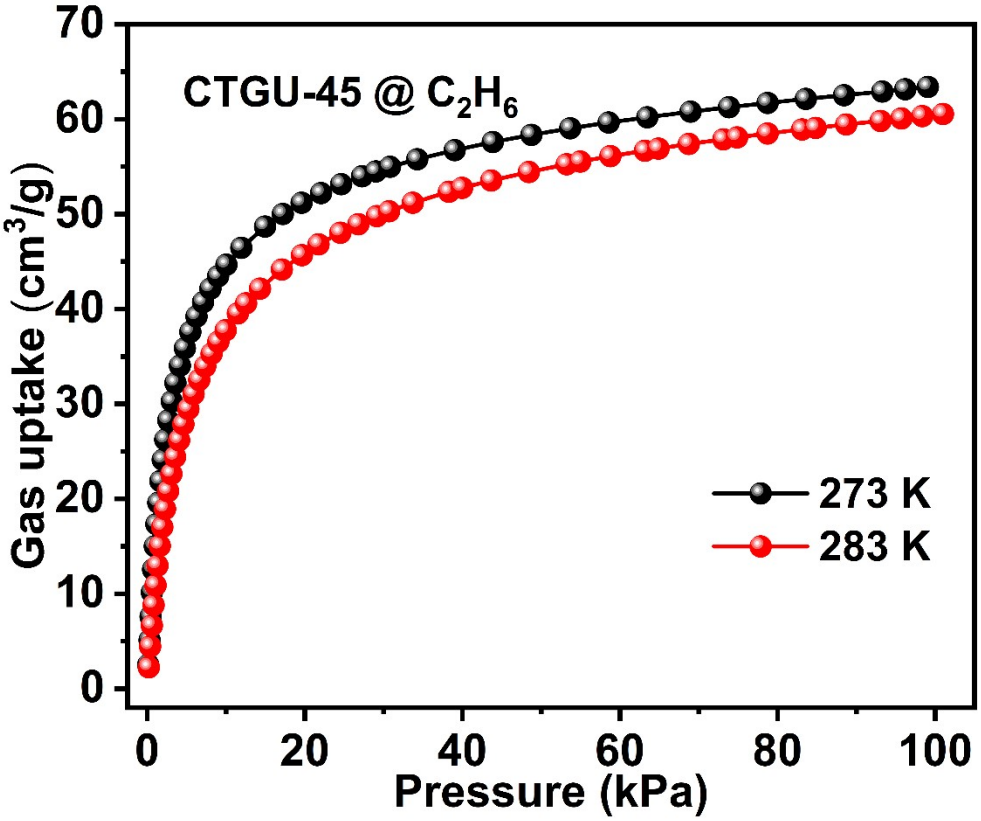

Figure S11. The adsorption isotherms of C_2H_6 in CTGU-45 at 273 , 283 K.

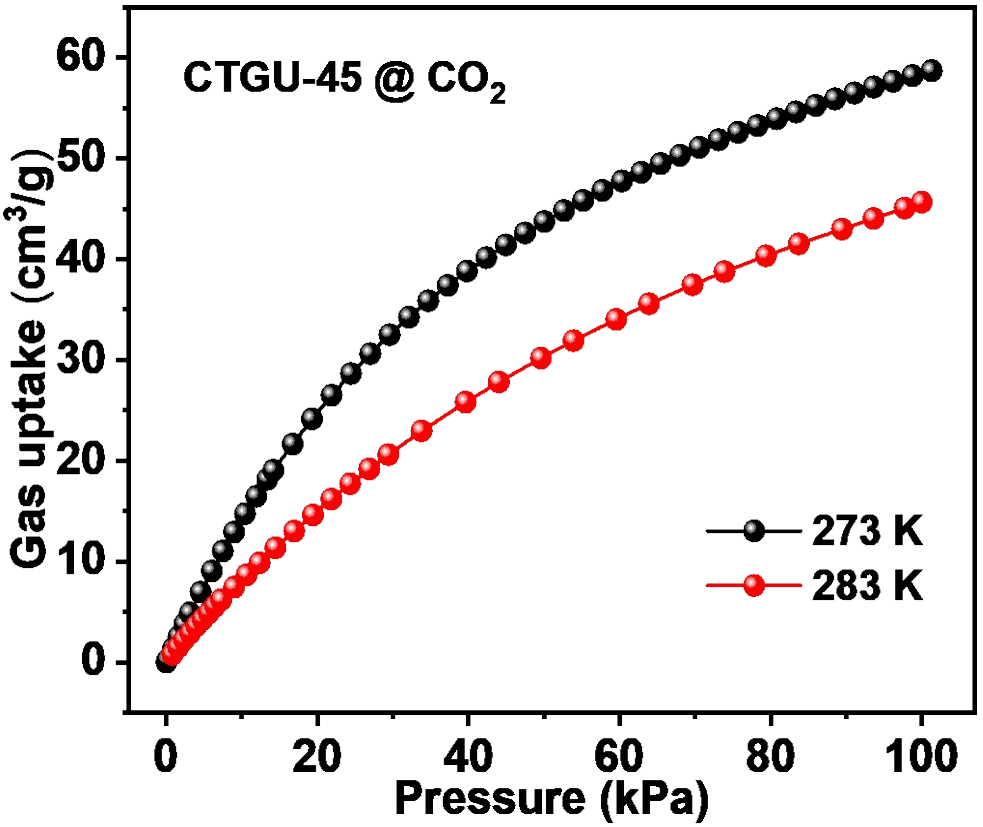

Figure S12. The adsorption isotherms of CO_2 in CTGU-45 at 273 , 283 K.

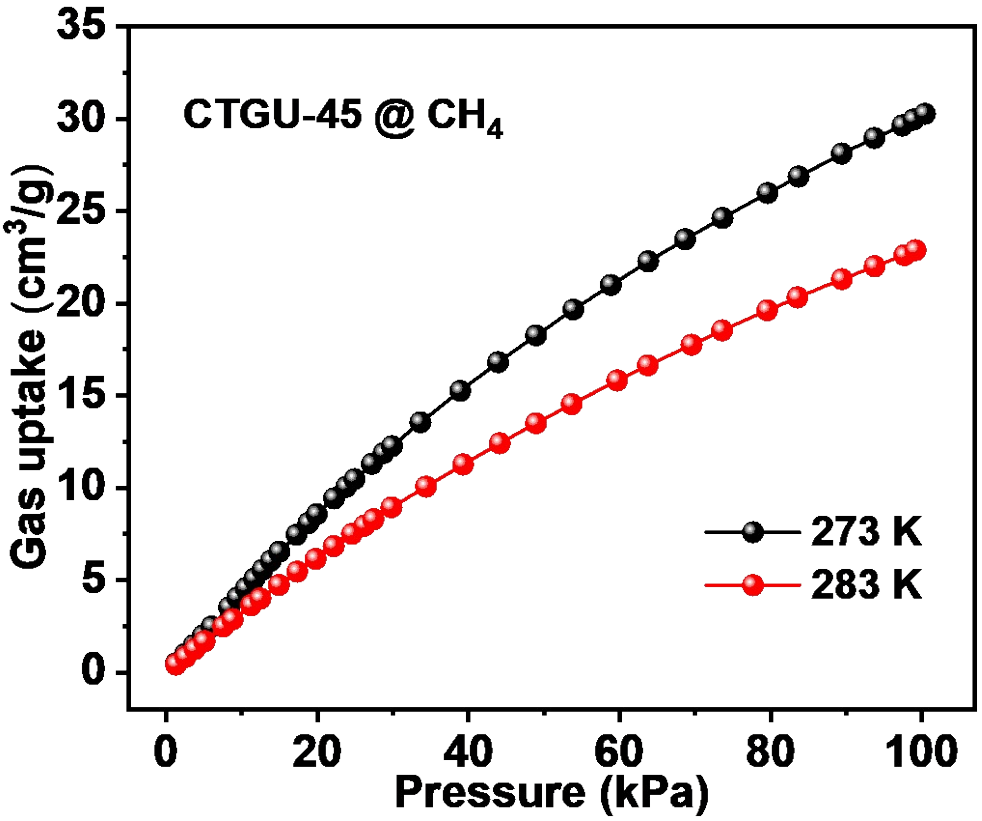

Figure S13. The adsorption isotherms of CH_4 in CTGU-45 at 273 , 283 K.

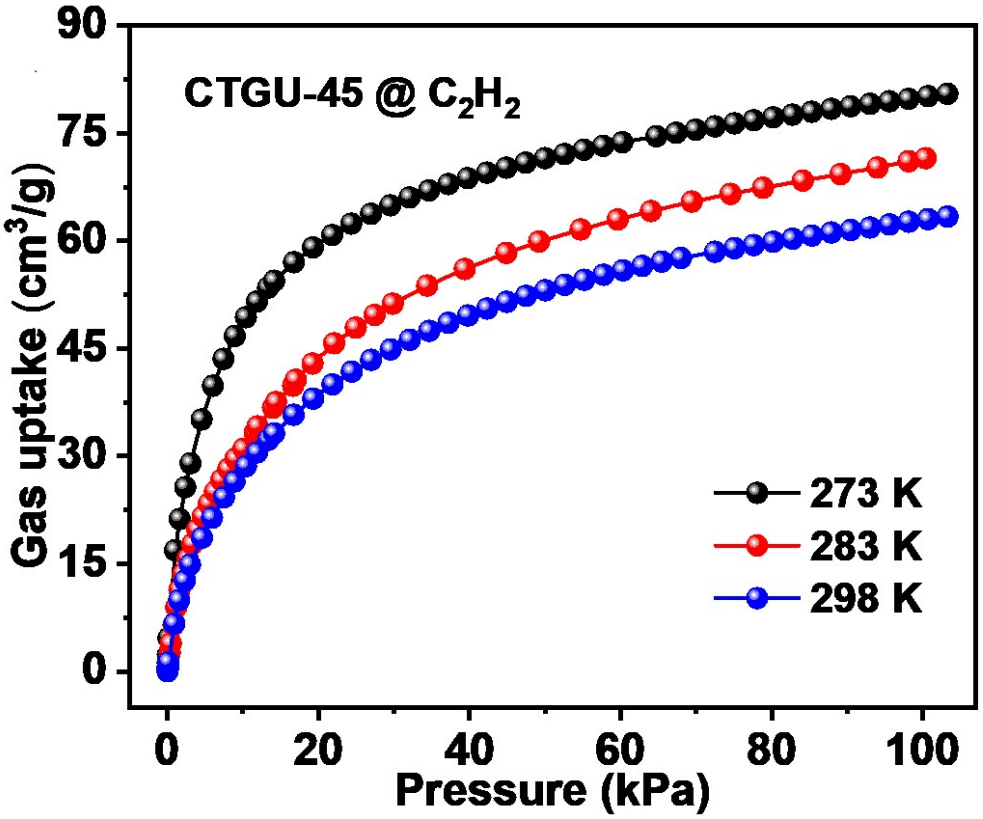

Figure S14. The adsorption isotherms of C_2H_2 in CTGU-45 at 273 , 283, and 298 K.

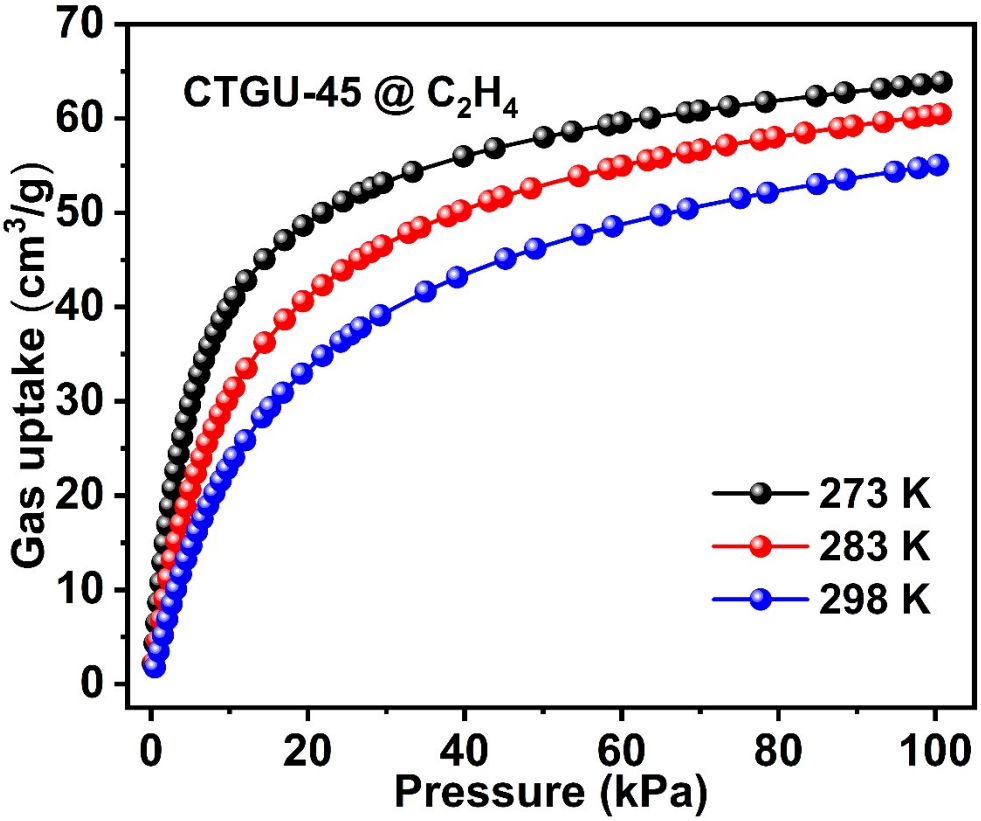

Figure S15. The adsorption isotherms of C_2H_4 in CTGU-45 at 273 , 283, and 298 K.

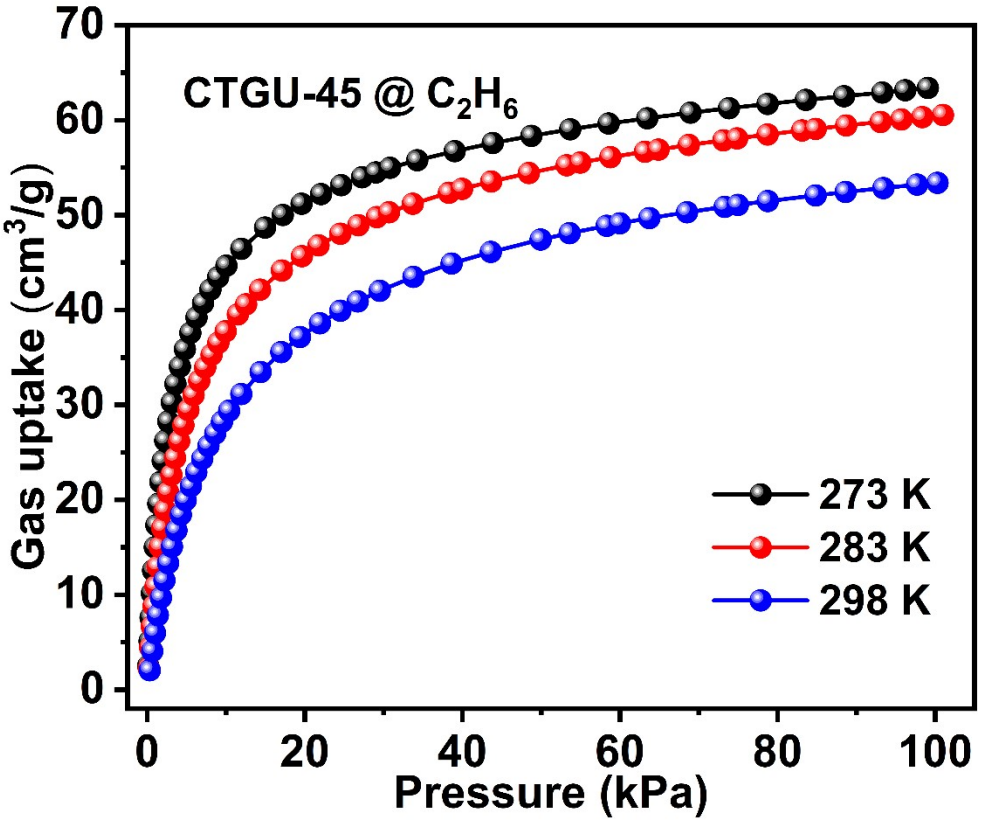

Figure S16. The adsorption isotherms of C_2H_6 in CTGU-45 at 273 , 283, and 298 K.

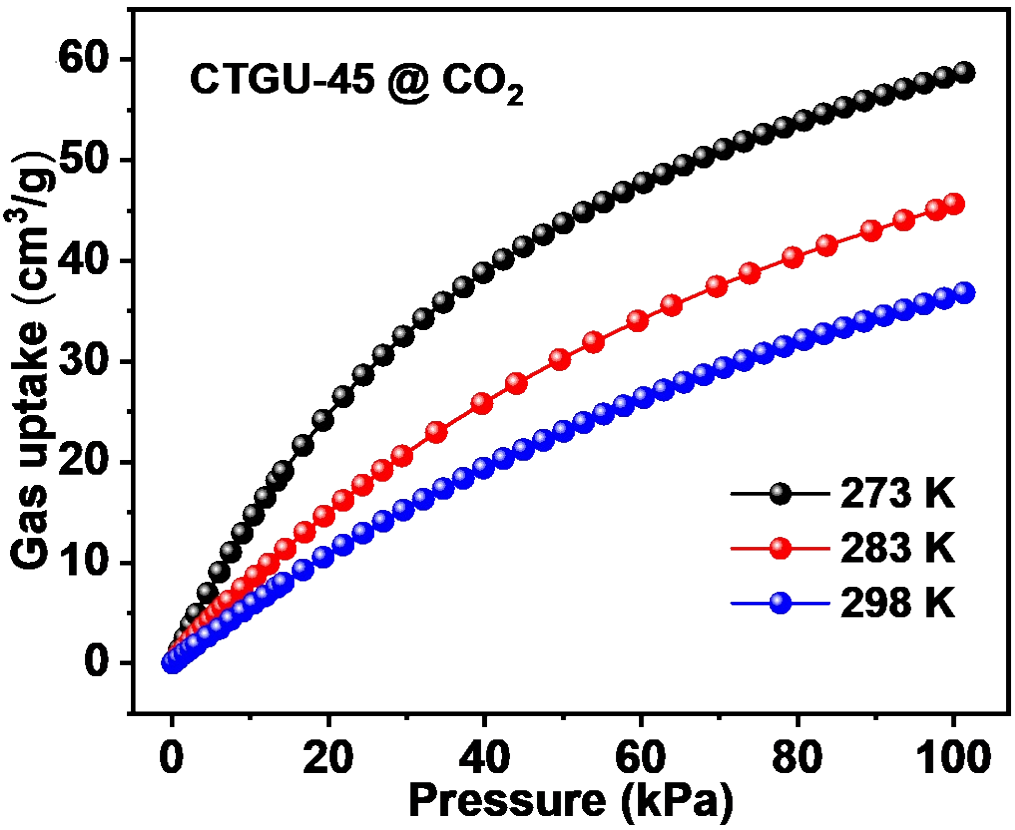

Figure S17. The adsorption isotherms of CO_2 in CTGU-45 at 273 , 283, and 298 K.

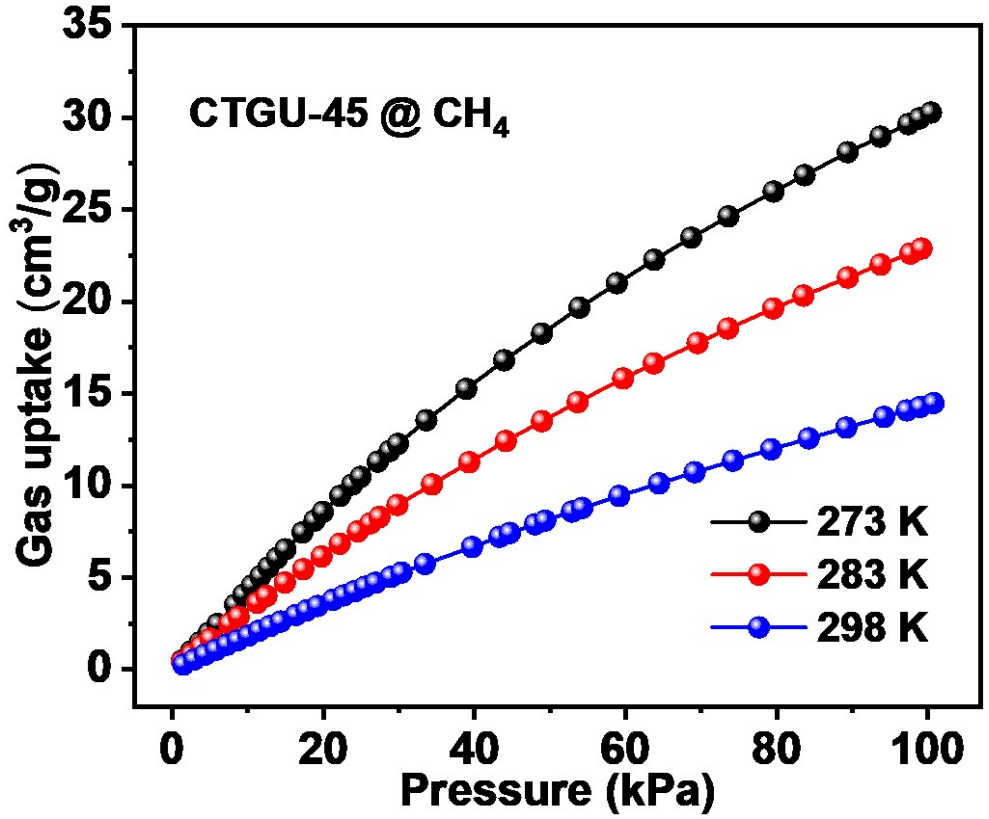

Figure S18. The adsorption isotherms of CH_4 in CTGU-45 at 273 , 283, and 298 K.

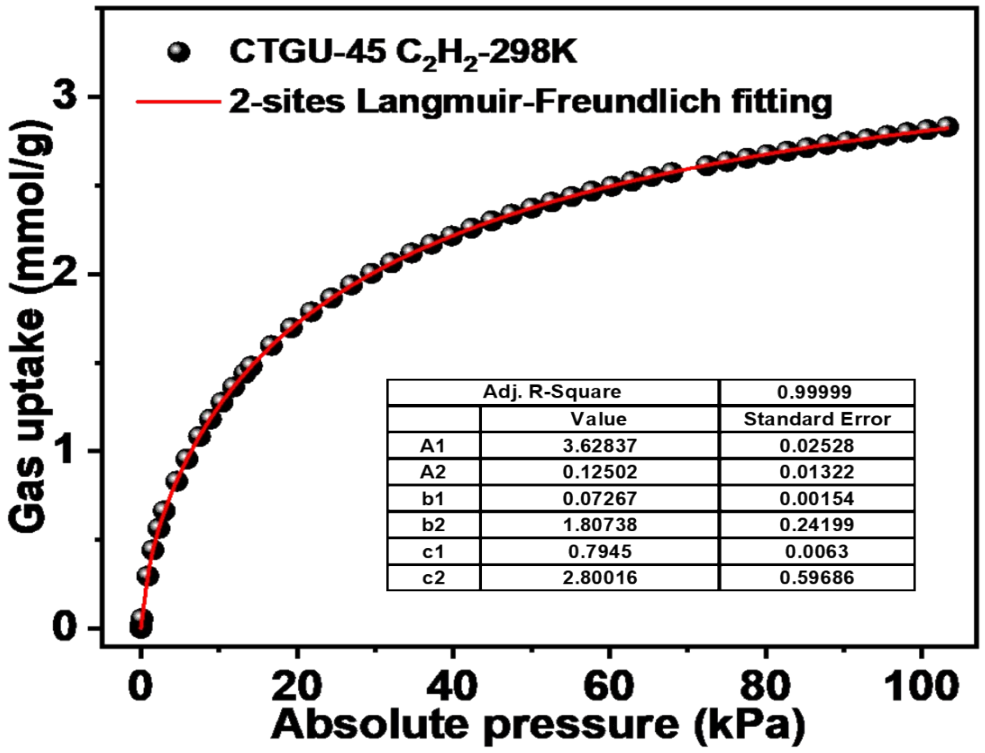

Adj. R-Square		0.99999
	Value	Standard Error
A1	3.62837	0.02528
A2	0.12502	0.01322
b1	0.07267	0.00154
b2	1.80738	0.24199
c1	0.7945	0.0063
c2	2.80016	0.59686

Figure S19. C_2H_2 adsorption isotherms at 298 K in CTGU-45 with dual-sites Langmuir-Freundlich model fits.

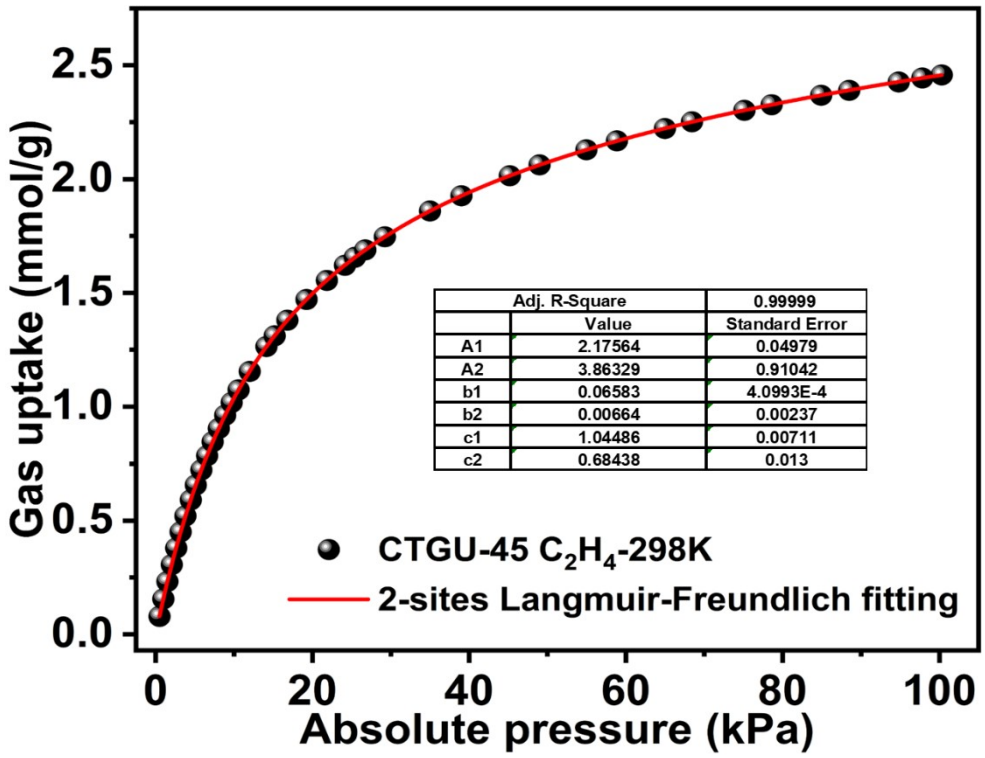

Adj. R-Square		0.99999
	Value	Standard Error
A1	2.17564	0.04979
A2	3.86329	0.91042
b1	0.06583	4.0993E-4
b2	0.00664	0.00237
c1	1.04486	0.00711
c2	0.68438	0.013

Figure S20. C_2H_4 adsorption isotherms at 298 K in CTGU-45 with dual-sites Langmuir-Freundlich model fits.

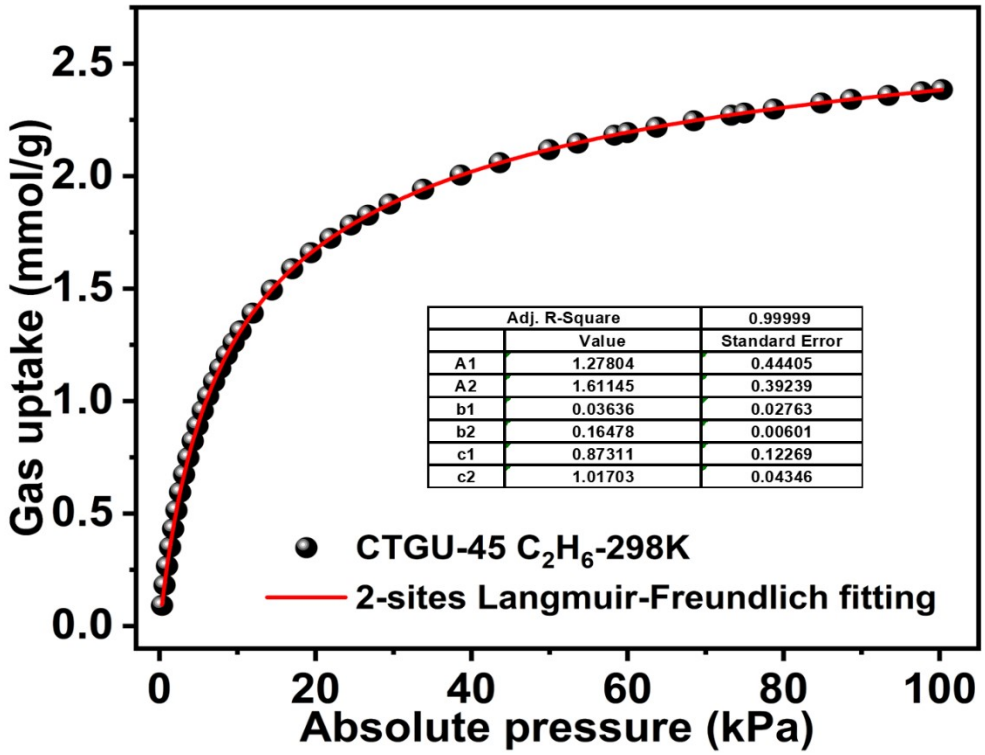

Figure S21. C_2H_6 adsorption isotherms at 298 K in CTGU-45 with dual-sites Langmuir-Freundlich model fits.

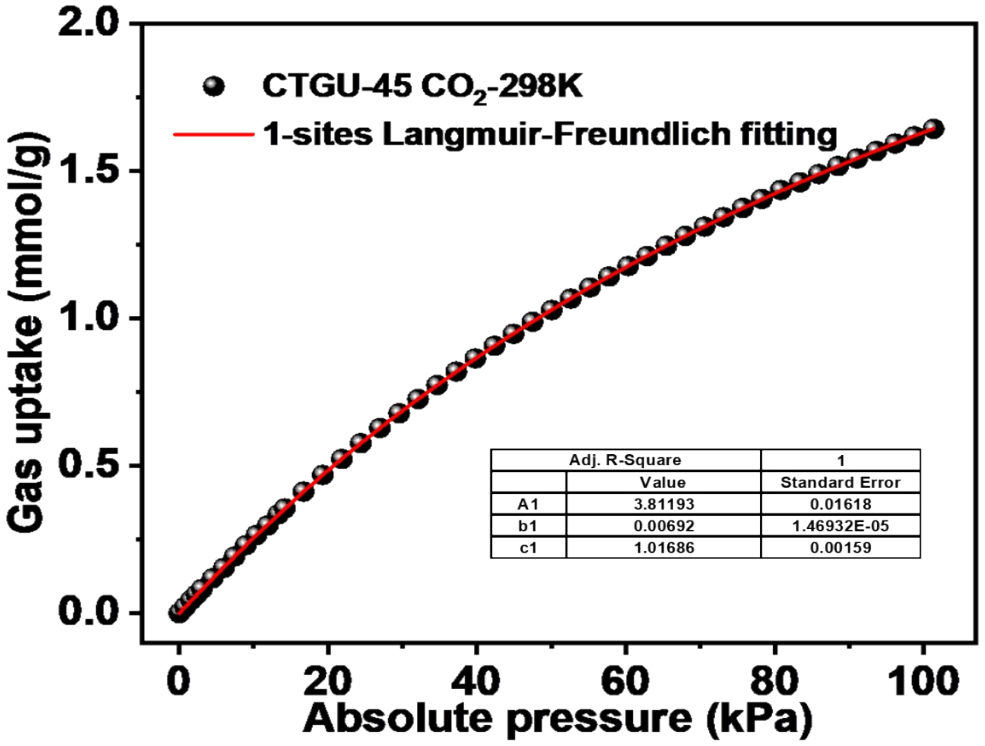

Figure S22. CO_2 adsorption isotherms at 298 K in CTGU-45 with single -site Langmuir-Freundlich model fits.

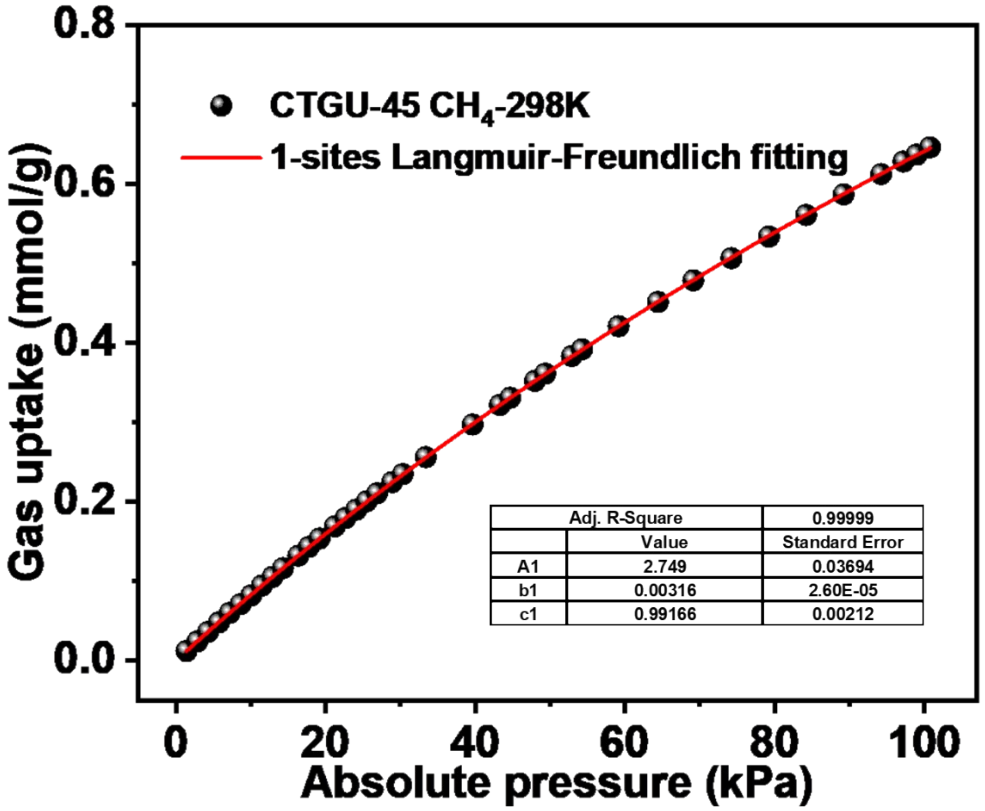

Figure S23. CH_4 adsorption isotherms at 298 K in CTGU-45 with single -site Langmuir-Freundlich model fits.

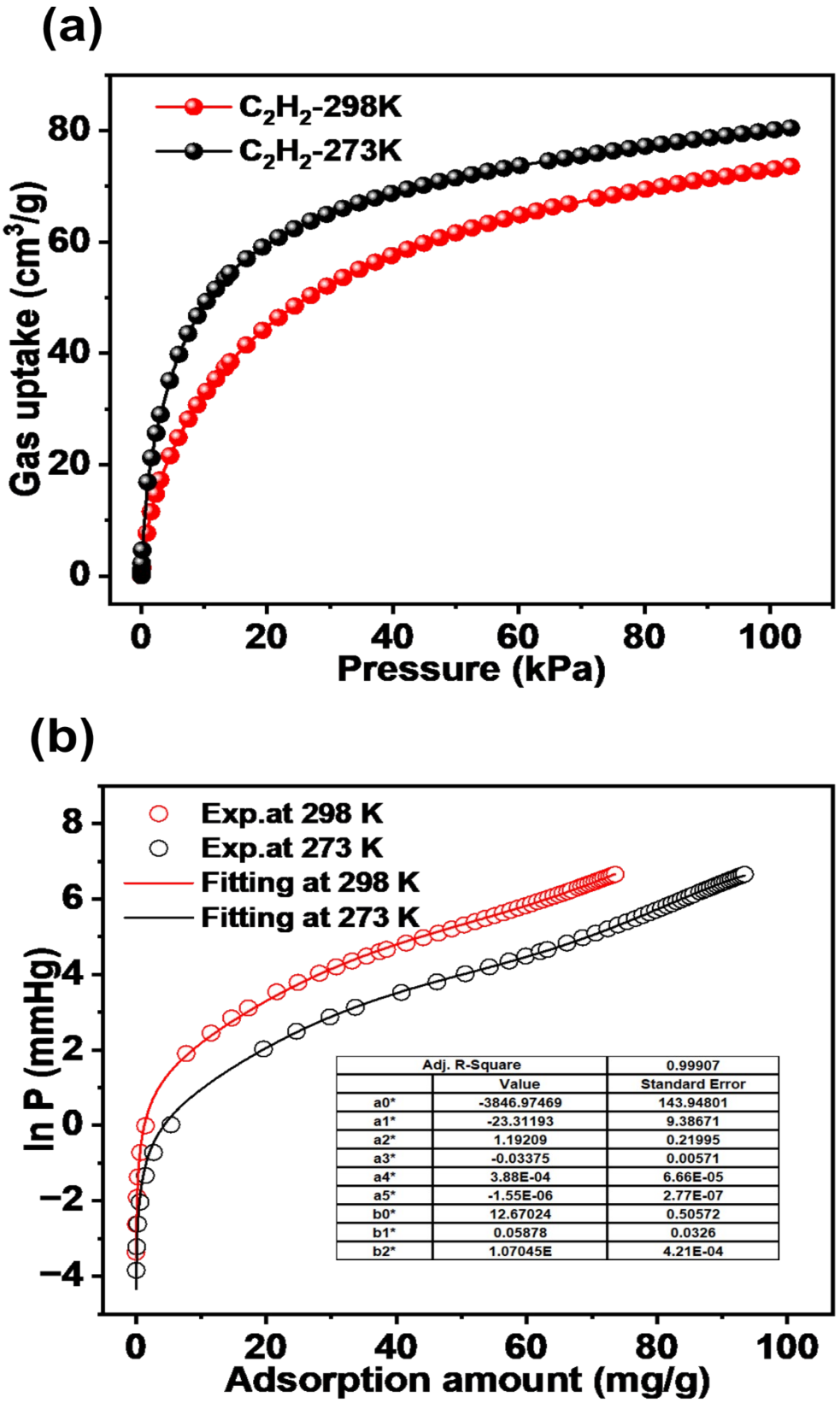

Figure S24. Virial fitting of (a) C_2H_2 adsorption isotherms of CTGU-45 for Q_{st} calculation. The fitting parameters are listed in the picture (inset). Isosteric heat of adsorption of (b) C_2H_2 on CTGU-45.

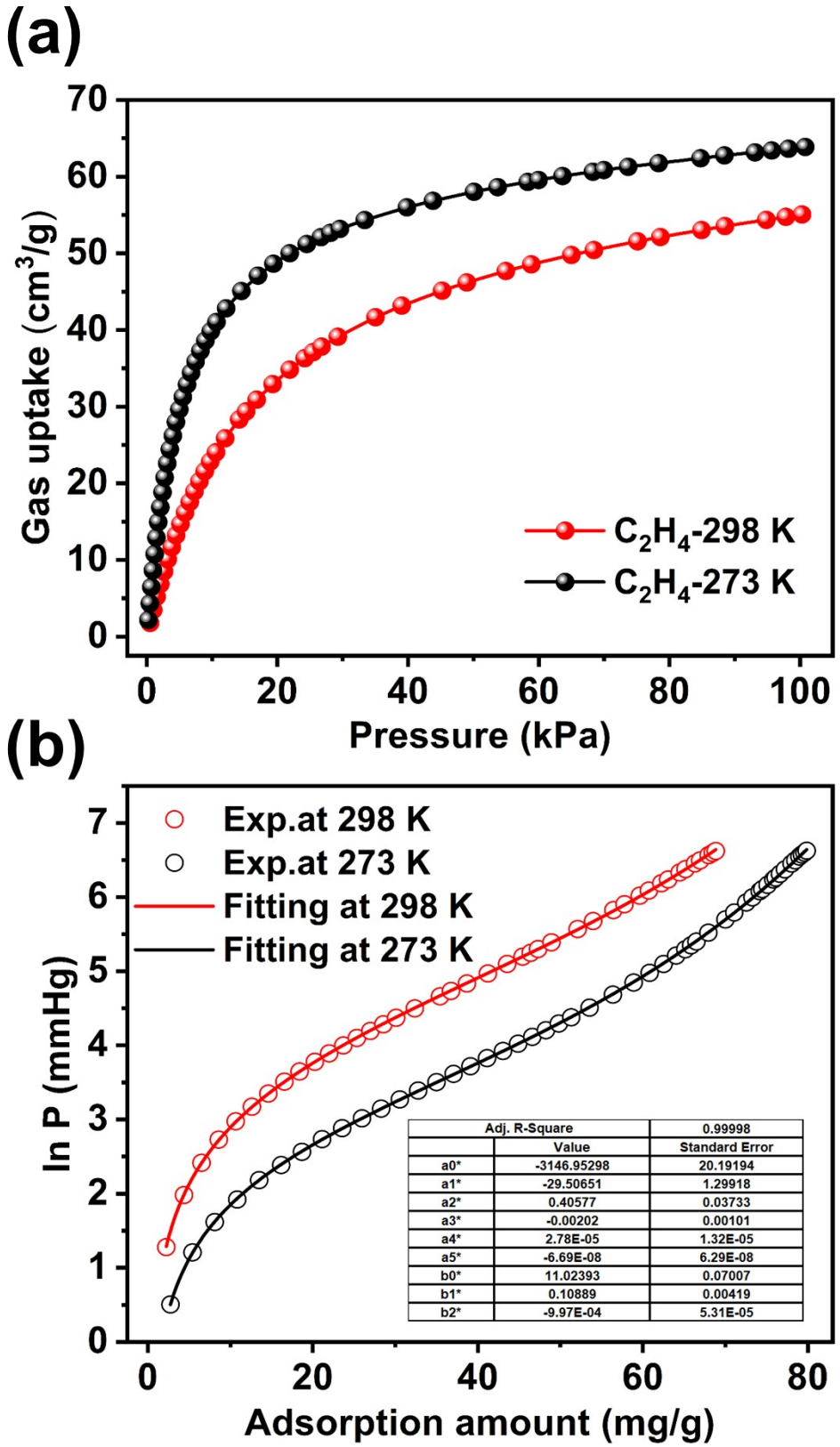

Figure S25. Virial fitting of (a) C_2H_4 adsorption isotherms of CTGU-45 for Q_{st} calculation. The fitting parameters are listed in the picture (inset). Isosteric heat of adsorption of (b) C_2H_4 on CTGU-45.

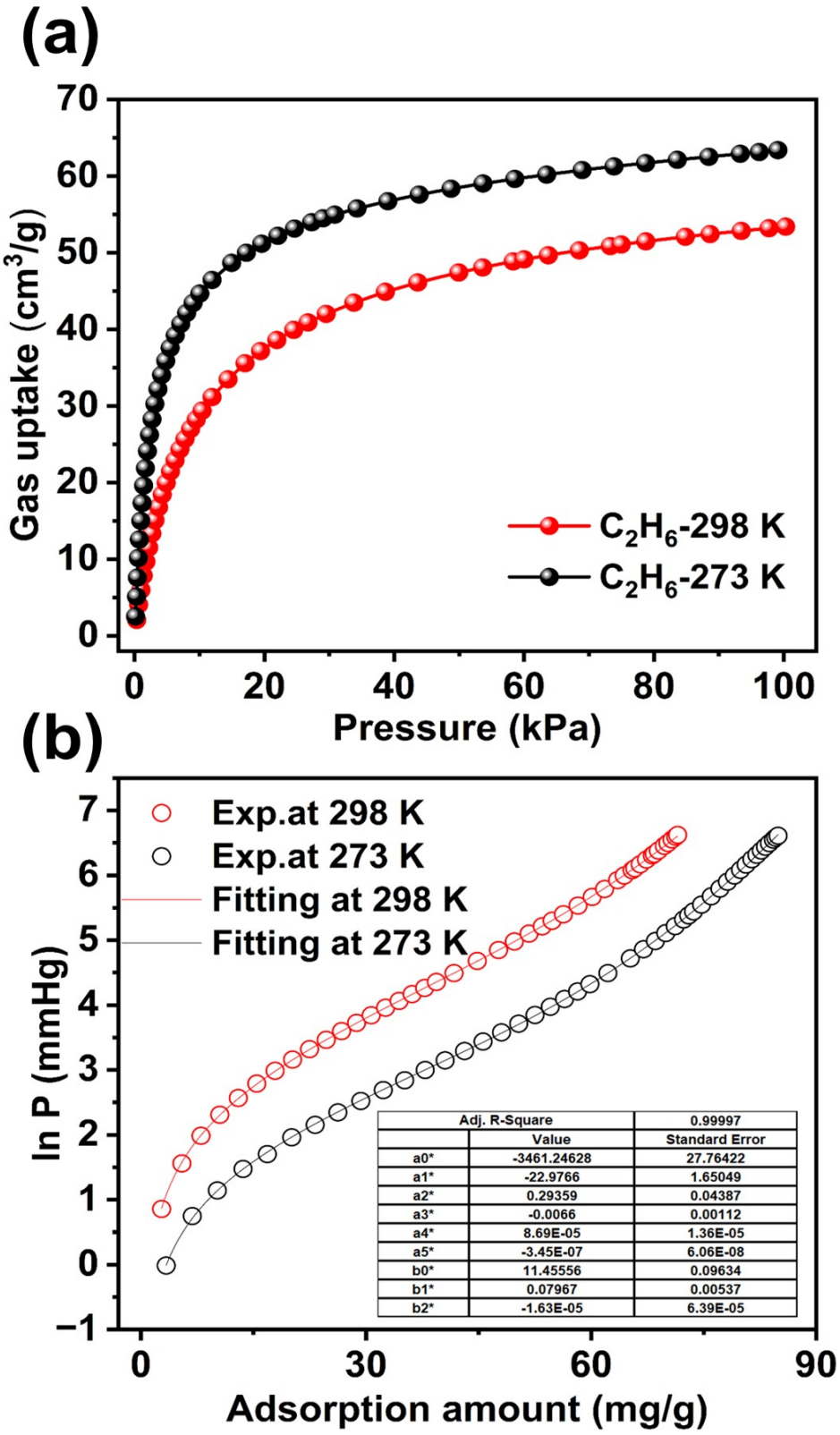

Figure S26. Virial fitting of (a) C_2H_6 adsorption isotherms of CTGU-45 for Q_{st} calculation. The fitting parameters are listed in the picture (inset). Isosteric heat of adsorption of (b) C_2H_6 on CTGU-45.

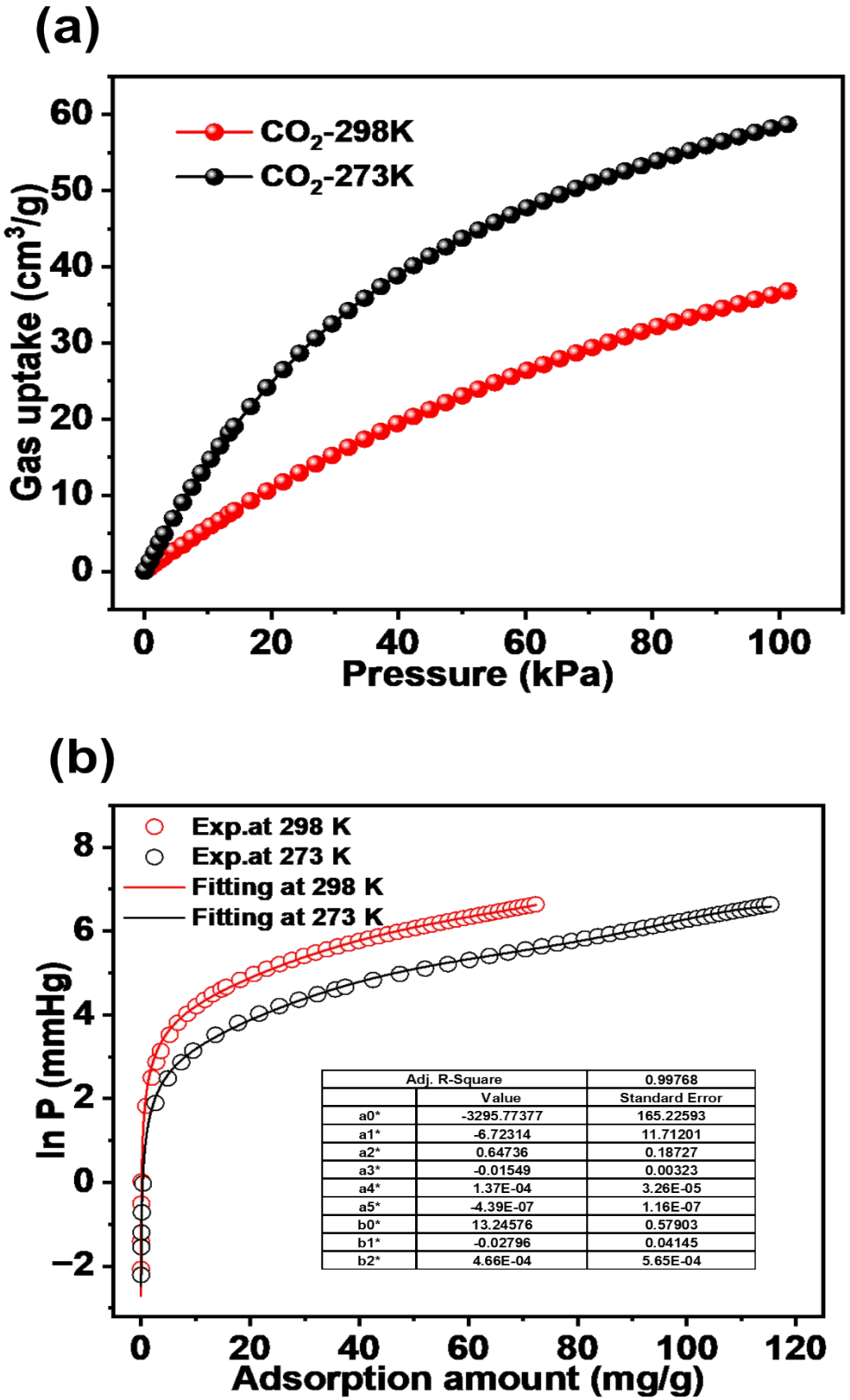

Adj. R-Square		0.99768
	Value	Standard Error
a0*	-3295.77377	165.22593
a1*	-6.72314	11.71201
a2*	0.64736	0.18727
a3*	-0.01549	0.00323
a4*	1.37E-04	3.26E-05
a5*	-4.39E-07	1.16E-07
b0*	13.24576	0.57903
b1*	-0.02796	0.04145
b2*	4.66E-04	5.65E-04

Figure S27. Virial fitting of (a) CO_2 adsorption isotherms of CTGU-45 for Q_{st} calculation. The fitting parameters are listed in the picture (inset). Isosteric heat of adsorption of (b) CO_2 on CTGU-45.

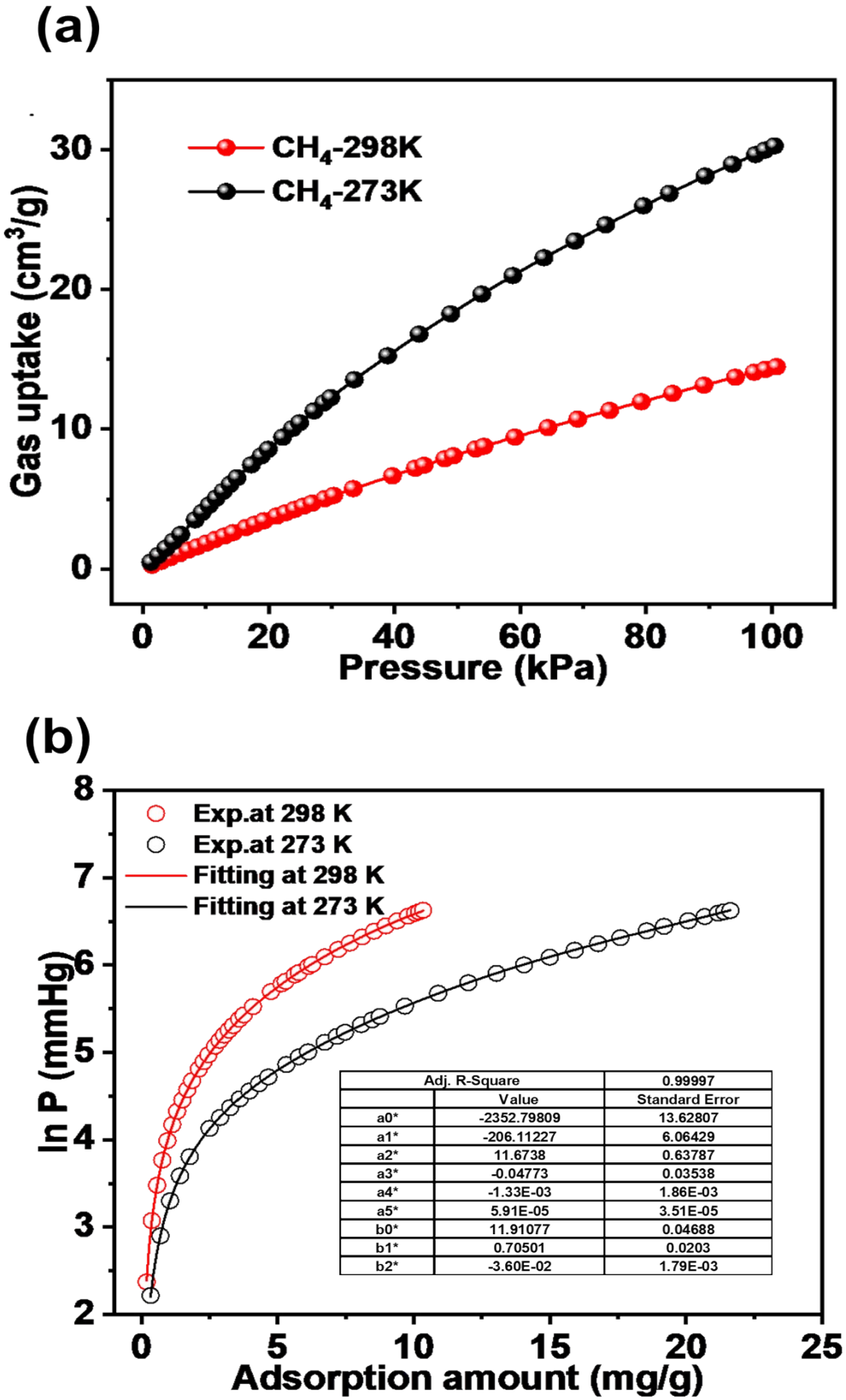

Adj. R-Square		0.99997
	Value	Standard Error
a0*	-2352.79809	13.62807
a1*	-206.11227	6.06429
a2*	11.6738	0.63787
a3*	-0.04773	0.03538
a4*	-1.33E-03	1.86E-03
a5*	5.91E-05	3.51E-05
b0*	11.91077	0.04688
b1*	0.70501	0.0203
b2*	-3.60E-02	1.79E-03

Figure S28. Virial fitting of (a) CH_4 adsorption isotherms of CTGU-45 for Q_{st} calculation. The fitting parameters are listed in the picture (inset). Isosteric heat of adsorption of (b) CH_4 on CTGU-45.

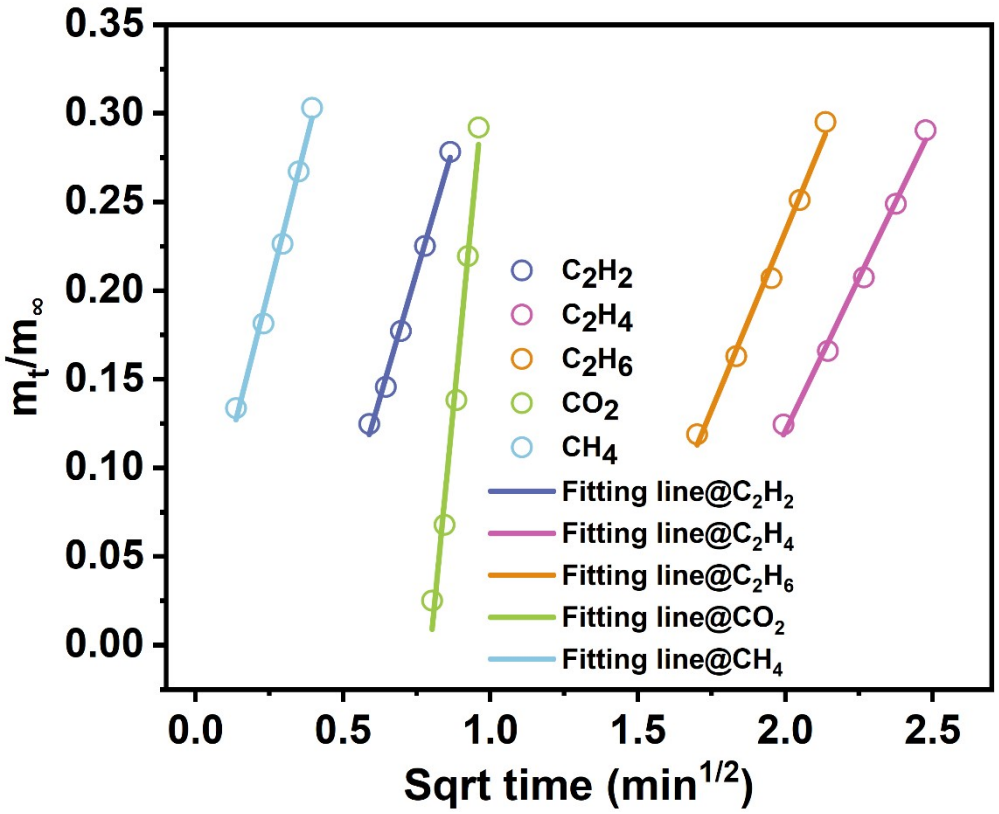

CTGU-48	C_2H_2	CO_2	CH_4	C_2H_4	C_2H_6
Diffusion time constants, D_C/r_c^2 , s^{-1}	0.0284	0.2628	0.0380	0.0104	0.0141
R^2	0.9929	0.9798	0.9886	0.9933	0.9920

Figure S29. The fitting of diffusion time constants based on the profiles of C_2H_2, C_2H_4, C_2H_6, CO_2, and CH_4 for CTGU-48, and the calculated diffusion time constants and R^2.

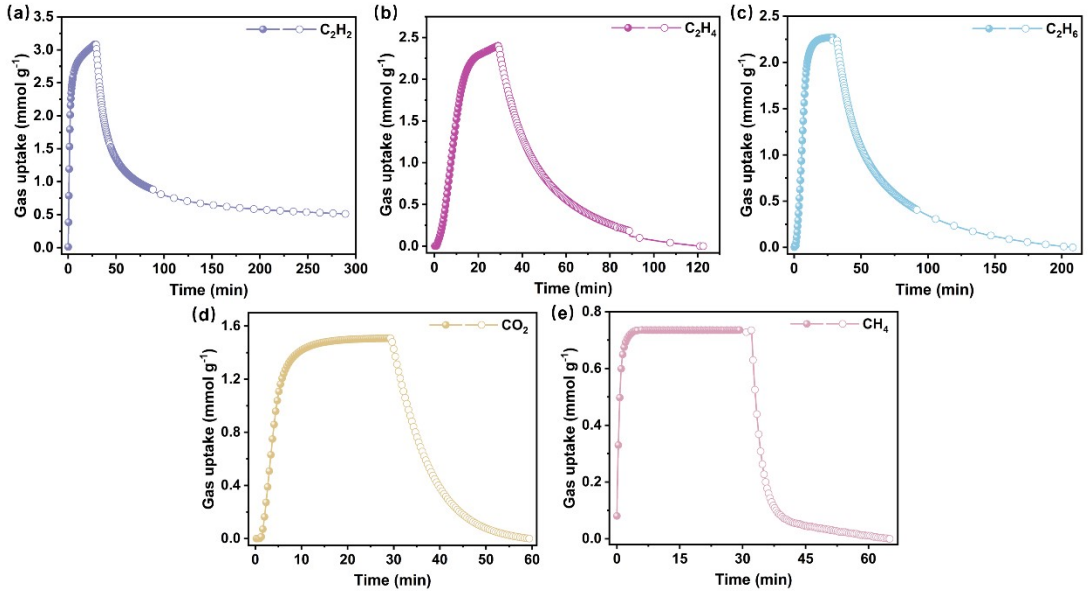

Figure S30. Adsorption/desorption kinetics profiles of CTGU-45 for C_2H_2, C_2H_4, C_2H_6, CO_2, and CH_4.

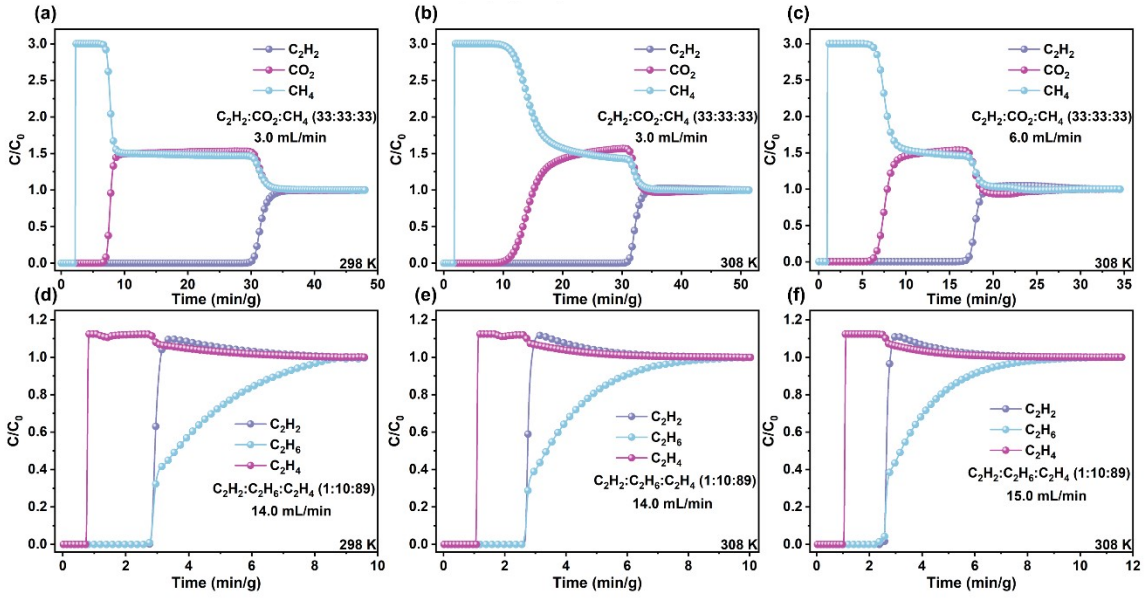

Figure S31. Experimental column breakthrough curves for (a-c) $C_2H_2/CO_2/CH_4$ (33/33/33, v/v/v) and (d-f) $C_2H_2/C_2H_6/C_2H_4$ (1/10/89, v/v/v) on CTGU-45 at 298 and 308 K with different total flow rates.

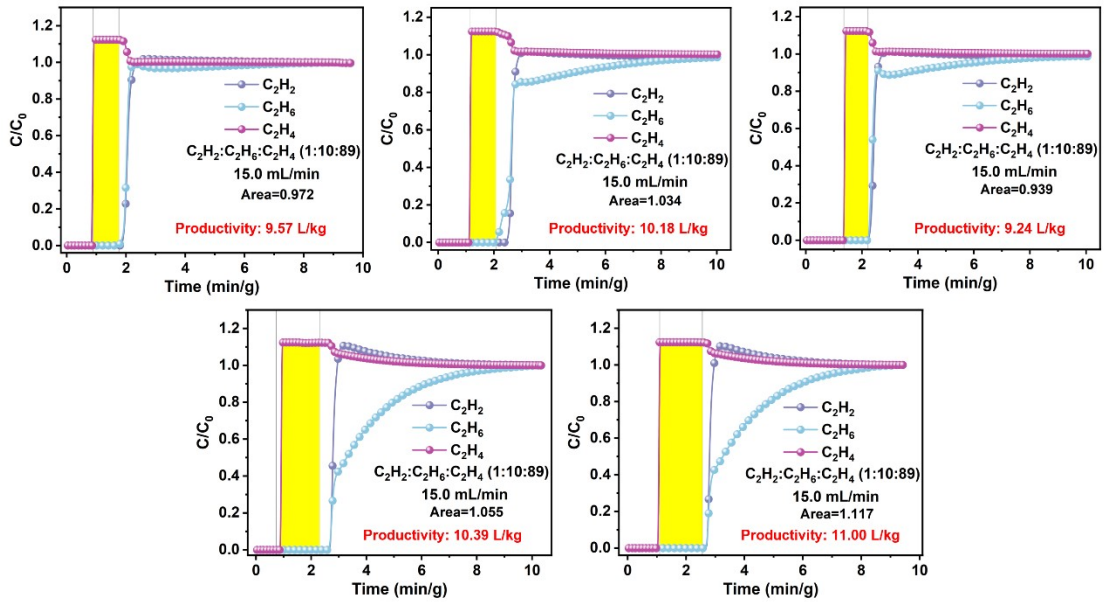

Figure S32. Breakthrough cycling test of CTGU-45 for $C_2H_2/C_2H_6/C_2H_4$ (1:10:89) at 298 K under a total flow rate of 15 mL min^{-1}.

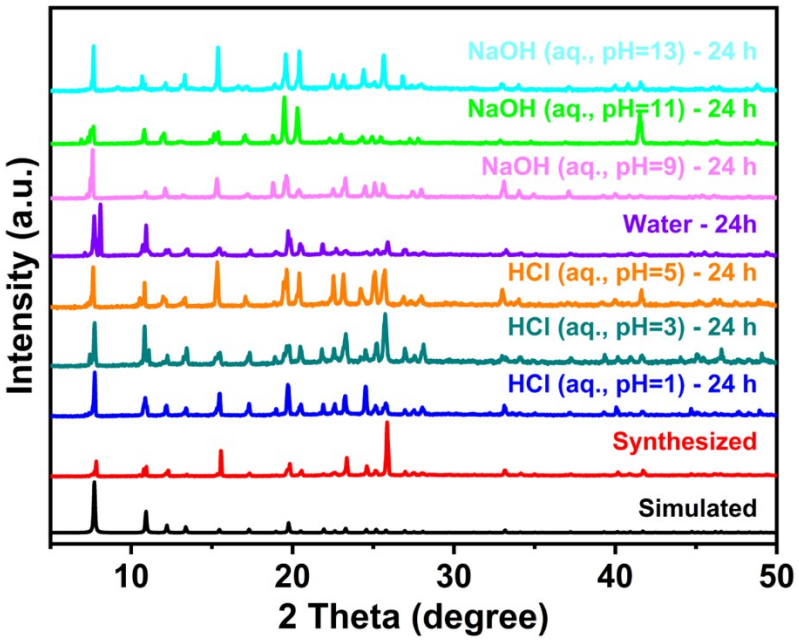

Figure S33. PXRD patterns of CTGU-45 after treatment with acidic or alkaline aqueous solution.

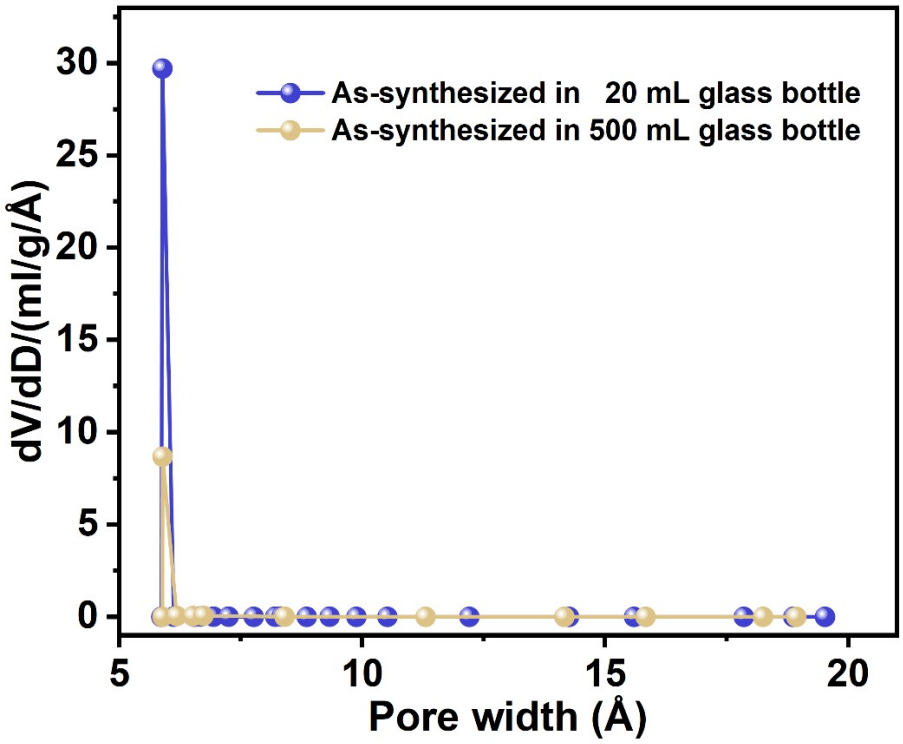

Figure S34. Pore size distributions of the CTGU-45 samples prepared at 500-mL and 20-mL scales obtained from the N_2 ads/desorption data (77 K).

Table S2. Comparison of the Anion-Pillared MOFs on C_2H_2 and CO_2 adsorption capacity, IAST selectivity of C_2H_2/CO_2, and adsorption enthalpy (Q_{st}).

Porous Materials	C_2H_2 uptake (cm^3/g)	CO_2 uptake (cm^3/g)	IAST selectivity (50:50)	Q_{st} (C_2H_2) (kJ/mol)	Q_{st} (CO_2) (kJ/mol)	Refs
CTGU-45	**63.38**	**36.81**	**5.66**	**31.99**	**27.40**	**This work**
SIFSIX-Cu-TPA	185.20	107.30	5.3	39.1	25.7	[10]
QDU-MOF-1	141.03	127.76	2.95	72.52	39.89	[11]
MPM-1-TIFSIX	101.47	86.91	0.83	30.1	48.4	[12]
TIFSIX-17-Ni	73.92	49.28	21	48.3	37.8	[13]
NBOFFIVE-dps-Cu	36.96	24.64	9	53.6	/	[14]
sql-SIFSIX-bpe-Zn	40	/	8.4	67.5	33.6	[15]
SIFSIX-DPA-Cu-i	75.59	22.5	9.34	46.53	26.36	[16]
SIFSIX-17-Ni	73.92	51.52	11.7	44.2	40.2	[13]
SIFSIX-pyz-SH-Ni	75.94	49.95	10	41.5	35.5	[17]
DICRO-4-Ni-I	43.01	23.07	14	37.7	33.9	[18]

TIFSIX-2-Cu-I	91.84	96.32	6.5	46.3	35.8	[19]
ZNU-8	113.12	49.73	3.74	27.2	23.4	[20]
ZNU-9	117.86	96.77	10.3	33.1	26.6	[20]
ZNU-12	176.52	96.98	13.35	36.08	31.89	[21]
ZNU-15	36.0	13.5	10.5	54.0	42.8	[22]
BSF-2	41.44	29.79	5.1	37.3	28.7	[23]
BSF-4	53.31	35.84	9.8	35	24.5	[24]
NBOFFIVE-3-Ni	85.12	42.56	6	36.7	25.0	[25]

Table S3. Summary of adsorption performance for one-step C_2H_4 purification materials at 298 K.

Porous Materials	C_2H_2 uptake (mmol/g)	C_2H_4 uptake (mmol/g)	C_2H_6 uptake (mmol/g)	IAST selectivity (50:50)	Q_{st} (C_2H_2) (kJ/mol)	Q_{st} (C_2H_4) (kJ/mol)	Q_{st} (C_2H_6) (kJ/mol)	Ref.
CTGU-45	**2.83**	**2.46**	**2.38**	**5.66**	**31.99**	**25.80**	**27.3**	
Zn-trz-ox	2.67	2.43	2.49	2.5	36.8	32.7	38.7	[26]
NUM-9	1.98[c]	1.79[c]	2.06[c]	1.61	35.79	32.32	35.75	[27]
Zr-TCA	2.78	2.02	2.28	2.72	43.8	23.9	35.3	[28]
ZUL-100	3.62	2.42	2.82	2.12[b]	36.5	29.6	34.2	[29]
ZSTU-2	3.11	2.35	2.73	1.62	23.5	32	33.5	[30]
Zn-atz-oba	2.77	2.03	2.04	1.27	27.5	27.0	30.0	[31]
NPU-1	5.1	4.2	4.5	1.32	27.88	23.95	29.1	[32]
TJT-100	4.46	3.44	3.70	1.2	31	25	29	[33]
Azole-Th-1	3.51	3.56	4.42	1.46	25.4	26.1	28.6	[34]
BUT-321	4.09	3.33	3.56	1.6	25.0	28.2	28.5	[35]
ZJNU-115	4.73	3.75	4.2	1.56	29.2	27.7	28.2	[36]
HIAM-326	2.91	1.85	2.28	1.9	24.98	23.39	27.54	[37]
MOF-303	7.94	5.00	5.00	1.7	31.7	24.3	25.1	[38-39]
MUV-11	3.98	1.72	1.83	1.53	20.3	23.5	25	[30]

References

1. Sheldrick, G. M. Crystal Structure Refinement with Shelxl. *Acta Crystallogr. C* **2015**, *71,* 3-8.

2. Dolomanov, O.; Bourhis, L.; Gildea, R.; Howard, J.; Puschmann, H. Olex2: A Complete Structure Solution, Refinement and Analysis Program. *J. Appl. Cryst.* **2009**, *42,* 339-341.

3. Myers, A. L.; Prausnitz, J. M. Thermodynamics of Mixed-Gas Adsorption. *AIChE J.* **1965**, *11,* 121-127.

4. Hand, D. W.; Loper, S.; Ari, M.; Crittenden, J. C. Prediction of Multicomponent Adsorption Equilibria Using Ideal Adsorbed Solution Theory. *Environ. Sci. Technol.* **1985**, *19,* 1037-1043.

5. Czepirski, L.; JagieŁŁo, J. Virial-Type Thermal Equation of Gas—Solid Adsorption. *Chem. Eng. Sci.* **1989**, *44,* 797-801.

6. Fang, Y.; Bai, X.; Zhang, X.; Li, J.-R. Data-Driven Discovery of Metal–Organic Frameworks for Sieving Separation of Quinary C_5 Olefin Mixtures. *J. Am. Chem. Soc.* **2025**, *147,* 42016-42023.

7. Lee, K.; Howe, J. D.; Lin, L.-C.; Smit, B.; Neaton, J. B. Small-Molecule Adsorption in Open-Site Metal–Organic Frameworks: A Systematic Density Functional Theory Study for Rational Design. *Chem. Mater.* **2015**, *27,* 668-678.

8. Grimme, S. Semiempirical Gga-Type Density Functional Constructed with a Long-

Range Dispersion Correction. *J. Comput. Chem.* **2006**, *27,* 1787-1799.

9. Yang, H.; Wang, Y.; Krishna, R.; Jia, X.; Wang, Y.; Hong, A. N.; Dang, C.; Castillo, H. E.; Bu, X.; Feng, P. Pore-Space-Partition-Enabled Exceptional Ethane Uptake and Ethane-Selective Ethane–Ethylene Separation. *J. Am. Chem. Soc.* **2020**, *142,* 2222-2227.

10. Li, H.; Liu, C.; Chen, C.; Di, Z.; Yuan, D.; Pang, J.; Wei, W.; Wu, M.; Hong, M. An Unprecedented Pillar-Cage Fluorinated Hybrid Porous Framework with Highly Efficient Acetylene Storage and Separation. *Angew. Chem. Int. Edit.* **2021**, *60,* 7547-7552.

11. Li, H.-Y.; Xue, Z.-Z.; Han, S.-D.; Wang, G.-M.; He, T. A Microporous Fluorinated MOF for Efficient Separation of C_2H_2 from C_2H_2/CO_2 and C_2H_2/C_2H_4 Mixtures. *Sep. Purif. Technol.* **2025**, *357,* 130094.

12. Nugent, P. S.; Rhodus, V. L.; Pham, T.; Forrest, K.; Wojtas, L.; Space, B.; Zaworotko, M. J. A Robust Molecular Porous Material with High CO_2 Uptake and Selectivity. *J. Am. Chem. Soc.* **2013**, *135,* 10950-10953.

13. Mukherjee, S.; Kumar, N.; Bezrukov, A. A.; Tan, K.; Pham, T.; Forrest, K. A.; Oyekan, K. A.; Qazvini, O. T.; Madden, D. G.; Space, B.; Zaworotko, M. J. Amino-Functionalised Hybrid Ultramicroporous Materials That Enable Single-Step Ethylene Purification from a Ternary Mixture. *Angew. Chem. Int. Edit.* **2021**, *60,* 10902-10909.

14. Shivanna, M.; Otake, K.-i.; Song, B.-Q.; van Wyk, L. M.; Yang, Q.-Y.; Kumar, N.; Feldmann, W. K.; Pham, T.; Suepaul, S.; Space, B.; Barbour, L. J.; Kitagawa, S.; Zaworotko, M. J. Benchmark Acetylene Binding Affinity and Separation through Induced

Fit in a Flexible Hybrid Ultramicroporous Material. *Angew. Chem. Int. Edit.* **2021**, *60,* 20383-20390.

15. Gao, M.-Y.; Bezrukov, A. A.; Song, B.-Q.; He, M.; Nikkhah, S. J.; Wang, S.-Q.; Kumar, N.; Darwish, S.; Sensharma, D.; Deng, C.; Li, J.; Liu, L.; Krishna, R.; Vandichel, M.; Yang, S.; Zaworotko, M. J. Highly Productive C_3H_4/C_3H_6 Trace Separation by a Packing Polymorph of a Layered Hybrid Ultramicroporous Material. *J. Am. Chem. Soc.* **2023**, *145,* 11837-11845.

16. You, J.; Wang, H.; Xiao, T.; Wu, X.; Zhang, L.; Lu, C.-Z. Introducing High Concentration of Hexafluorosilicate Anions into an Ultra-Microporous MOF for Highly Efficient C_2H_2/CO_2 and C_2H_2/C_2H_4 Separation. *Chem. Eng. J.* **2023**, *477,* 147001.

17. Wen, H.-M.; Liao, C.; Li, L.; Yang, L.; Wang, J.; Huang, L.; Li, B.; Chen, B.; Hu, J. Reversing C_2H_2–CO_2 Adsorption Selectivity in an Ultramicroporous Metal–Organic Framework Platform. *Chem. Commun.* **2019**, *55,* 11354-11357.

18. Scott, H. S.; Shivanna, M.; Bajpai, A.; Madden, D. G.; Chen, K.-J.; Pham, T.; Forrest, K. A.; Hogan, A.; Space, B.; Perry Iv, J. J.; Zaworotko, M. J. Highly Selective Separation of C_2H_2 from CO_2 by a New Dichromate-Based Hybrid Ultramicroporous Material. *ACS Appl. Mater. Interfaces.* **2017**, *9,* 33395-33400.

19. Chen, K.-J.; Scott, Hayley S.; Madden, David G.; Pham, T.; Kumar, A.; Bajpai, A.; Lusi, M.; Forrest, Katherine A.; Space, B.; Perry, John J.; Zaworotko, Michael J. Benchmark C_2H_2/CO_2 and CO_2/C_2H_2 Separation by Two Closely Related Hybrid

Ultramicroporous Materials. *Chem* **2016**, *1,* 753-765.

20. Zhang, Y.; Sun, W.; Luan, B.; Li, J.; Luo, D.; Jiang, Y.; Wang, L.; Chen, B. Topological Design of Unprecedented Metal-Organic Frameworks Featuring Multiple Anion Functionalities and Hierarchical Porosity for Benchmark Acetylene Separation. *Angew. Chem. Int. Edit.* **2023**, *62,* e202309925.

21. Zhang, Y.; Han, Y.; Luan, B.; Wang, L.; Yang, W.; Jiang, Y.; Ben, T.; He, Y.; Chen, B. Metal–Organic Framework with Space-Partition Pores by Fluorinated Anions for Benchmark C_2H_2/CO_2 Separation. *J. Am. Chem. Soc.* **2024**, *146,* 17220-17229.

22. Chen, H.; He, Y.; Han, Y.; Hu, J.; Li, J.; Jiang, Y.; Keshta, B.; Wang, L.; Zhang, Y. A New Sifsix Anion Pillared Cage MOF with Crs Topological Structure for Efficient C_2H_2/CO_2 Separation. *Chin. J. Struct. Chem.* **2025**, *44,* 100508.

23. Zhang, Y.; Hu, J.; Krishna, R.; Wang, L.; Yang, L.; Cui, X.; Duttwyler, S.; Xing, H. Rational Design of Microporous MOFs with Anionic Boron Cluster Functionality and Cooperative Dihydrogen Binding Sites for Highly Selective Capture of Acetylene. *Angew. Chem. Int. Edit.* **2020**, *59,* 17664-17669.

24. Wang, L.; Sun, W.; Zhang, Y.; Xu, N.; Krishna, R.; Hu, J.; Jiang, Y.; He, Y.; Xing, H. Interpenetration Symmetry Control within Ultramicroporous Robust Boron Cluster Hybrid MOFs for Benchmark Purification of Acetylene from Carbon Dioxide. *Angew. Chem. Int. Edit.* **2021**, *60,* 22865-22870.

25. Kumar, N.; Mukherjee, S.; Harvey-Reid, N. C.; Bezrukov, A. A.; Tan, K.; Martins, V.;

Vandichel, M.; Pham, T.; van Wyk, L. M.; Oyekan, K.; Kumar, A.; Forrest, K. A.; Patil, K. M.; Barbour, L. J.; Space, B.; Huang, Y.; Kruger, P. E.; Zaworotko, M. J. Breaking the Trade-Off between Selectivity and Adsorption Capacity for Gas Separation. *Chem* **2021**, *7,* 3085-3098.

26. Wu, T.; Yu, C.; Krishna, R.; Qiu, Z.; Pan, H.; Zhang, P.; Suo, X.; Yang, L.; Cui, X.; Xing, H. Porous Materials with Suitable Pore Size and Dual-Functional Sites for Benchmark One-Step Ethylene Purification. *AIChE J.* **2024**, *70,* e18312.

27. Yang, S.-Q.; Sun, F.-Z.; Liu, P.; Li, L.; Krishna, R.; Zhang, Y.-H.; Li, Q.; Zhou, L.; Hu, T.-L. Efficient Purification of Ethylene from C_2 Hydrocarbons with an C_2H_6/C_2H_2-Selective Metal–Organic Framework. *ACS Appl. Mater. Interfaces* **2021**, *13,* 962-969.

28. Liu, Y.; Xiong, H.; Chen, J.; Chen, S.; Zhou, Z.; Zeng, Z.; Deng, S.; Wang, J. One-Step Ethylene Separation from Ternary C_2 Hydrocarbon Mixture with a Robust Zirconium Metal–Organic Framework. *Chin. J. Chem. Eng.* **2023**, *59,* 9-15.

29. Zhang, P.; Zhong, Y.; Zhang, Y.; Zhu, Z.; Liu, Y.; Su, Y.; Chen, J.; Chen, S.; Zeng, Z.; Xing, H.; Deng, S.; Wang, J. Synergistic Binding Sites in a Hybrid Ultramicroporous Material for One-Step Ethylene Purification from Ternary C_2 Hydrocarbon Mixtures. *Sci. Adv. 8,* eabn9231.

30. Liu, P.; Wang, Y.; Chen, Y.; Yang, J.; Wang, X.; Li, L.; Li, J. Construction of Saturated Coordination Titanium-Based Metal–Organic Framework for One-Step $C_2H_2/C_2H_6/C_2H_4$ Separation. *Sep. Purif. Technol.* **2021**, *276,* 119284.

31. Cao, J.-W.; Mukherjee, S.; Pham, T.; Wang, Y.; Wang, T.; Zhang, T.; Jiang, X.; Tang, H.-J.; Forrest, K. A.; Space, B.; Zaworotko, M. J.; Chen, K.-J. One-Step Ethylene Production from a Four-Component Gas Mixture by a Single Physisorbent. *Nat. Commun.* **2021**, *12,* 6507.

32. Zhu, B.; Cao, J.-W.; Mukherjee, S.; Pham, T.; Zhang, T.; Wang, T.; Jiang, X.; Forrest, K. A.; Zaworotko, M. J.; Chen, K.-J. Pore Engineering for One-Step Ethylene Purification from a Three-Component Hydrocarbon Mixture. *J. Am. Chem. Soc.* **2021**, *143,* 1485-1492.

33. Hao, H.-G.; Zhao, Y.-F.; Chen, D.-M.; Yu, J.-M.; Tan, K.; Ma, S.; Chabal, Y.; Zhang, Z.-M.; Dou, J.-M.; Xiao, Z.-H.; Day, G.; Zhou, H.-C.; Lu, T.-B. Simultaneous Trapping of C_2H_2 and C_2H_6 from a Ternary Mixture of $C_2H_2/C_2H_4/C_2H_6$ in a Robust Metal–Organic Framework for the Purification of C_2H_4. *Angew. Chem. Int. Edit.* **2018**, *57,* 16067-16071.

34. Xu, Z.; Xiong, X.; Xiong, J.; Krishna, R.; Li, L.; Fan, Y.; Luo, F.; Chen, B. A Robust Th-Azole Framework for Highly Efficient Purification of C_2H_4 from a $C_2H_4/C_2H_2/C_2H_6$ Mixture. *Nat. Commun.* **2020**, *11,* 3163.

35. Zhang, P.-D.; Wu, X.-Q.; Shuai, Q.; Yu, J.; Zhang, X.; Li, J.-R. Optimizing the Microenvironment of Pores in an MOF for Boosting Ethylene Purification from a Ternary-Component Mixture. *ACS Mater. Lett* **2024**, *6,* 4632-4638.

36. Fan, L.; Zhou, P.; Wang, X.; Yue, L.; Li, L.; He, Y. Rational Construction and Performance Regulation of an In(Ⅲ)–Tetraisophthalate Framework for One-Step

Adsorption-Phase Purification of C_2H_4 from C_2 Hydrocarbons. *Inorg. Chem.* **2021**, *60,* 10819-10829.

37. Liu, J.; Zhou, K.; Ullah, S.; Miao, J.; Wang, H.; Thonhauser, T.; Li, J. Precise Pore Engineering of *Fcu*-Type Y-MOFs for One-Step C_2H_4 Purification from Ternary $C_2H_6/C_2H_4/C_2H_2$ Mixtures. *Small* **2023**, *19,* 2304460.

38. Wen, H.-M.; Yu, C.; Liu, M.; Lin, C.; Zhao, B.; Wu, H.; Zhou, W.; Chen, B.; Hu, J. Construction of Negative Electrostatic Pore Environments in a Scalable, Stable and Low-Cost Metal-Organic Framework for One-Step Ethylene Purification from Ternary Mixtures. *Angew. Chem. Int. Edit.* **2023**, *62,* e202309108.

39. Xian, S.; Peng, J.; Pandey, H.; Graham, W.; Yu, L.; Wang, H.; Tan, K.; Thonhauser, T.; Li, J. Simultaneous Removal of C_2H_2 and C_2H_6 for C_2H_4 Purification by Robust Mofs Featuring a High Density of Heteroatoms. *J. Mater. Chem. A* **2023**, *11,* 21401-21410.